*J. Fluid Mech.* (2006), *vol.* 556, *pp.* 227–251. © 2006 Cambridge University Press 
doi:10.1017/S0022112006009591 Printed in the United Kingdom

# A variational approach to ice stream flow

By CHRISTIAN SCHOOF

Department of Earth and Ocean Sciences, University of British Columbia, 6339 Stores Road, Vancouver, BC, V6T 1Z4, Canada
cschoof@eos.ubc.ca

(Received 24 February 2005 and in revised form 4 November 2005)

Ice sheets are susceptible to the formation of ice streams, or narrow bands of fast-flowing ice whose high velocities are caused by rapid sliding at the contact between ice and the underlying bed. Based on recent geophysical work which has shown that the sliding motion of ice streams may be described by a Coulomb friction law, we investigate how the location of ice streams depends on the geometry of an ice sheet and on the mechanical properties of the underlying bed. More generally, this problem is relevant to the flow of thin films with Coulomb (or 'solid') friction laws applied at their base. By analogy with friction problems in elasticity, we construct a variational formulation for the free boundary between ice streams, where bed failure occurs, and the surrounding ice ridges, where there is little or no sliding. This variational problem takes the form of a non-coercive variational inequality, and we show that solutions exist provided a force and moment balance condition is satisfied. In that case, solutions are also unique except under certain specialized circumstances which are unlikely to arise for a real ice sheet. Further, we show how the variational formulation of the ice flow problem can be exploited to calculate numerical solutions, and to simulate the effect of changing ice geometry and bed friction on the location and velocities of streaming flow. Lastly, we study the effect of ice-shelf buttressing on the flow of ice streams whose spatial extent is determined by the yield stress distribution of the bed. In line with previous studies of ice-shelf buttressing, we find that the removal of an ice shelf can cause an ice stream feeding the ice shelf to speed up considerably, which underlines the important role ice shelves may play in controlling the dynamics of marine ice sheets.

## 1. Introduction

The large-scale dynamics of land-based ice sheets, such as those covering Greenland and Antarctica, can usually be identified with the behaviour of a highly viscous thin film spreading under its own weight. Many practical ice sheet simulation models exploit this fact by using a classical lubrication or *shallow ice* approximation (Morland & Johnson 1980). 'Shallow' is, of course, a relative measure based on aspect ratio, as ice sheets are typically a kilometre thick and hundreds to thousands of kilometres wide.

A peculiar behaviour exhibited by ice sheets, which sets them apart from other geophysical thin-film flows, is the formation of ice streams. These bands of fast-flowing ice within an ice sheet are typically around fifty kilometres wide and hundreds of kilometres long, and are surrounded by more slowly moving ice often termed ice ridges (e.g. Alley & Bindschadler 2001). The high flow velocities of ice streams generally cannot be explained by vertical shearing in the ice, as one would expect from a typical

https://doi.org/10.1017/S0022112006009591 Published online by Cambridge University Press

lubrication flow, but must be caused by rapid sliding at the contact between ice and the underlying bed.

Observational evidence has shown that the flow of many ice streams is indeed poorly described by a classical lubrication approximation, in the sense that friction at the bed is often significantly less than the shear stress (or *driving stress*) that a lubrication approximation would predict (e.g. Whillans & van der Veen 1997; Joughin, MacAyeal & Tulaczyk 2004). This is consistent with geophysical studies which have indicated that the basal sliding motion of ice streams is essentially a form of Coulomb slip associated with the mechanical failure of plastic subglacial sediments (e.g. Tulaczyk 1999). More specifically, friction at the bed is simply the yield stress of the underlying sediments, which is independent of sliding velocity and determined purely by the difference between normal stress at the bed (which is approximately hydrostatic) and porewater pressure in the subglacial sediments. Consequently, the shear stress experienced by at least part of the base of an ice stream must be less than the local driving stress, as the bed would otherwise be able to support the driving stress everywhere without any mechanical failure in the subglacial sediments, and no rapid sliding would occur.

As a result of the expected imbalance between basal friction and driving stress, longitudinal and lateral shear stresses associated with horizontal shearing in the ice must play a leading-order role in the force balance of ice streams (MacAyeal 1989), as is also the case for the floating ice shelves which often surround land-based ice sheets (e.g. Morland 1987). By contrast, the flow of ice ridges – where basal shear stress is below the yield stress of the bed – is generally well-described by the shallow-ice approximation, in which the stress field is dominated by vertical shear stresses and longitudinal and lateral shear stresses are higher-order corrections. In view of these different mechanical characteristics of ice ridges and ice streams, different leading-order models apply to streams and ridges, and an important component in ice sheet modelling is therefore the ability to predict where these different models should apply, that is, the ability to determine the spatial extent of ice stream and ice ridge flow. For a present day ice sheet, this question does not arise as we can observe where streaming flow is taking place (as is done for instance in Joughin *et al.* 2004). However, if we wish to study how ice sheets respond to changes in environmental conditions, for instance to the disintegration of an ice shelf (e.g. Schmeltz *et al.* 2002), then a model which is able to predict how the spatial extent of streaming flow is affected by these changes becomes necessary.

In this paper, we follow Schoof (2004) and assume that basal sliding velocities are insignificant when there is no mechanical failure at the bed, that is, when the shear stress at the base of the ice is below the yield stress of the bed. This allows us to identify ice ridges with regions of no slip, while we label as 'ice streams' those regions in which the yield stress of the bed is attained and sliding occurs. For a given ice sheet geometry and spatial distribution of basal yield stresses, the location of these regions is then not known *a priori* but must be determined as part of the solution. Similar free boundary problems, in which regions of slip and no slip must be determined along with stress and strain fields, are ubiquitous in elasticity theory, and this similarity has previously been explored in Schoof (2004, 2006) for unidirectional glacial flows. The purpose of the present paper is to extend the work in Schoof (2006) to the depth-integrated viscous flow models which are usually used to describe three-dimensional ice sheet flow, and to discuss the limitations faced by the analogy with the elastic case. Specifically, we develop a variational approach to determining the spatial extent and flow velocities of ice stream flow for a given ice sheet geometry and distribution

https://doi.org/10.1017/S0022112006009591 Published online by Cambridge University Press

of basal yield stresses, and discuss the problems of existence, uniqueness and stability of solutions. The variational formulation also leads directly to a numerical method for solving the ice flow problem, and we use this to study numerically the effect of ice shelves on the ice streams which serve as their tributaries.

## 2. The model

In this section, we consider the flow of ice streams within an ice sheet fringed by floating ice shelves, and describe the relevant coupling between ice ridges, ice streams and ice shelves. Our approach is based on depth-integrated viscous flow models justified by the low aspect ratios of ice streams, ice ridges and ice shelves. In order to simplify our task, we consider only the 'diagnostic' problem of determining the location of regions of streaming flow and their flow velocities. The dynamic evolution problem is deferred to future work.

We use horizontal Cartesian coordinates $(x, y) = (x_1, x_2)$ and consider an ice sheet (including its surrounding ice shelves) occupying a region $\Omega$ of the $(x, y)$-plane. The thickness of ice will in this paper be denoted by $h(x, y)$, and its surface elevation by $s(x, y)$. The bed elevation $b(x, y)$ is then $b = s - h$ where the ice is in contact with the bed, while for ice shelves we have only the constraint $b < s - h$. As the models which we consider are all depth-integrated, the vertical coordinate $z = x_3$ does not feature explicitly below, except in Appendix A. Regions of ice stream flow will be denoted by $\Omega_{\text{stream}}$, while ice ridges are $\Omega_{\text{ridge}}$ and ice shelves are $\Omega_{\text{shelf}}$. These regions are obviously disjoint, and their union is $\Omega$ (or rather, is dense in $\Omega$). Note that the extent of ice shelf flow is the entire region occupied by floating ice and is therefore known *a priori* for a given ice sheet geometry (determined by $s(x, y)$, $h(x, y)$ and $b(x, y)$), while the regions of ridge and stream flow are determined implicitly by ice sheet geometry and the yield strength of the bed. We assume that the boundary $\partial\Omega$ of the ice sheet is an ice shelf calving front, where the ice shelf is in contact with the open ocean. The remaining relevant boundaries between ice shelves, ice streams and ice ridges will be denoted in a self-explanatory way by $\Gamma_{\text{shelf-stream}}$, $\Gamma_{\text{stream-ridge}}$ and $\Gamma_{\text{shelf-ridge}}$ (see also figure 1).

### 2.1. *Ice sheet and shelf models*

Mechanically, ice shelves and ice streams behave as thin viscous membranes being stretched under the action of gravitational forces and, in the case of ice streams, of friction at the bed. At leading order, they are plug flows in which the horizontal component of velocity is independent of depth in the ice. Denoting the horizontal component of the velocity field by $\boldsymbol{u} = (u, v) = (u_1, u_2)$, where $u$ and $v$ are parallel to the $x$- and $y$-axes, respectively, $\boldsymbol{u}$ satisfies a depth-integrated version of Stokes' equations. For ice streams with Coulomb friction at the bed, we have (e.g. MacAyeal 1989; Joughin *et al.* 2004, see also Appendix A)

$$2\frac{\partial}{\partial x}\left[\nu h\left(2\frac{\partial u}{\partial x}+\frac{\partial v}{\partial y}\right)\right]+\frac{\partial}{\partial y}\left[\nu h\left(\frac{\partial u}{\partial y}+\frac{\partial v}{\partial x}\right)\right]-\rho g h\frac{\partial s}{\partial x}-\tau_c u/|\boldsymbol{u}|=0, \qquad (2.1)$$

$$2\frac{\partial}{\partial y}\left[\nu h\left(2\frac{\partial v}{\partial y}+\frac{\partial u}{\partial x}\right)\right]+\frac{\partial}{\partial x}\left[\nu h\left(\frac{\partial u}{\partial y}+\frac{\partial v}{\partial x}\right)\right]-\rho g h\frac{\partial s}{\partial y}-\tau_c v/|\boldsymbol{u}|=0, \qquad (2.2)$$

in $\Omega_{\text{stream}}$, where we assume that sliding occurs, so $|\boldsymbol{u}| = \sqrt{u^2 + v^2} > 0$.

The first two terms on the left-hand side of these equation essentially represent depth-integrated viscous stresses, where $\nu$ is ice viscosity, while the third term is a

https://doi.org/10.1017/S0022112006009591 Published online by Cambridge University Press

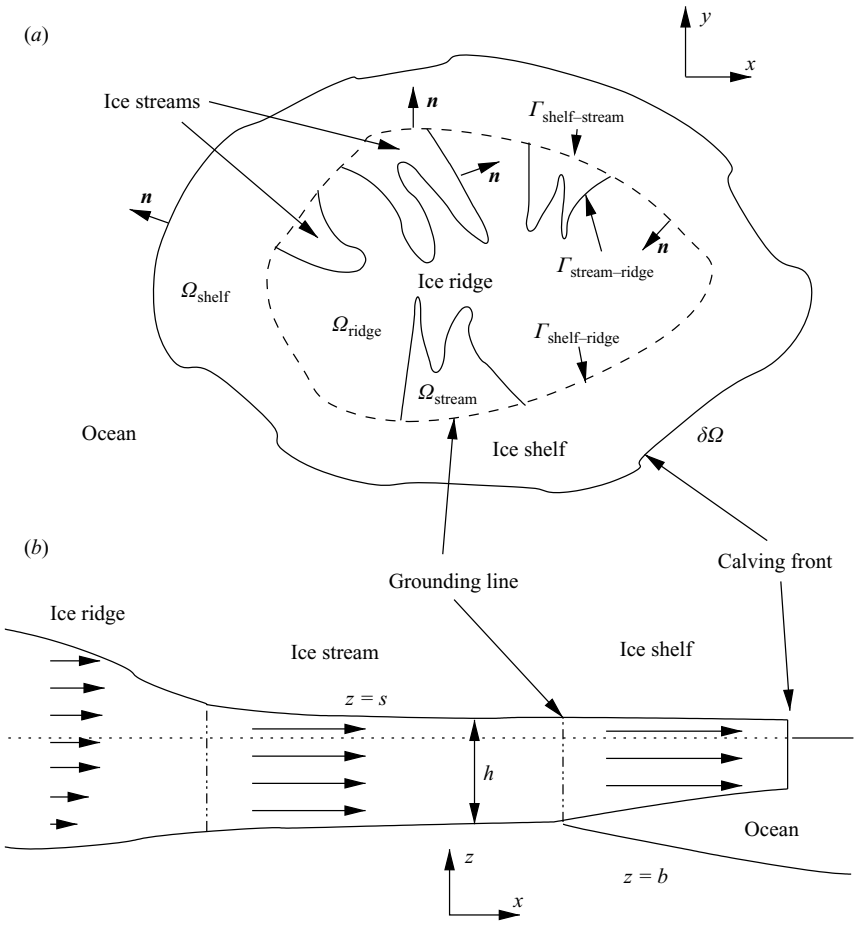



FIGURE 1. (*a*) Plan view of the domain and (*b*) a vertical cross-section of an ice ridge–ice stream–ice shelf sequence vertically exaggerated). In (*a*), the calving front of the ice shelf and the ice stream–ice ridge boundaries are shown as solid lines, while the grounding line is shown dashed. Normal vectors $\boldsymbol{n}$ are shown in the way they are used in the text. In (*b*), we have indicated the different vertical velocity profiles expected in ice ridges and ice streams by horizontal arrows.

gravitational driving force due to the surface slope of the ice stream, where $\rho$ is the density of ice and $g$ is acceleration due to gravity. More specifically, vertical force balance requires at leading order that pressure consists of a hydrostatic term and a dynamic term which balances vertical deviatoric stresses ($\tau_{33}$ in the notation of Appendix A). The gradient of pressure in the $x$-direction then accounts not only for the term $-\rho g h(\partial s/\partial x, \partial s/\partial y)$ in (2.1)–(2.2), but also for part of the first term on the left-hand side, as explained in Appendix A. Ice is typically taken to be a shear-thinning power-law material, and viscosity $\nu$ is given by

$$\nu = \frac{B}{2}\left[\frac{1}{2}\left(\frac{\partial u}{\partial x}\right)^2 + \frac{1}{2}\left(\frac{\partial v}{\partial y}\right)^2 + \frac{1}{2}\left(\frac{\partial u}{\partial x} + \frac{\partial v}{\partial y}\right)^2 + \frac{1}{4}\left(\frac{\partial u}{\partial y} + \frac{\partial v}{\partial x}\right)^2\right]^{(p-2)/2}, \quad (2.3)$$

where the third term inside the square brackets arises from replacing vertical compressive strain rate with the sum of horizontal compressive strain rates, as

https://doi.org/10.1017/S0022112006009591 Published online by Cambridge University Press

required by the incompressibility of ice. $B$ and $p$ are constants with $1 < p < 2$, and are related to the usual parameters $A$ and $n$ in Glen's law rheology for ice (Paterson 1994, chapter 5) by $B = A^{-1/n}$ and $p = 1 + 1/n$. Thus, for the widely used value $n = 3$, we obtain $p = 4/3$. The fourth term on the left-hand side of (2.1) is the $x$-component of basal friction, whose modulus $\tau_c$ is the failure strength of the subglacial sediment, and whose direction is opposite to the sliding velocity $\boldsymbol{u}$. The bed yield stress $\tau_c$ is given by

$$\tau_c = \mu(\rho g h - p_w), \tag{2.4}$$

where we assume that porewater pressure $p_w(x, y)$ at the base of the ice sheet is at or below the ice overburden $\rho g h$, while $\mu(x, y)$ is a positive friction coefficient which may vary spatially depending on the type of sediment at the ice stream bed. We assume $\mu$ and $p_w$ to be known functions of position. Hence $\tau_c$ is a known non-negative function and need not be determined as part of the solution (this fact is useful later in the construction of a variational formulation).

For ice shelves, (2.1) and (2.2) also apply, but with $\tau_c = 0$ (as there is no friction at the bed, see also Morland 1987; MacAyeal 1996). Also, the ice in ice sheets floats, so $s = (1 - \rho/\rho_w)h$, where $\rho_w$ is the density of water.

### 2.2. *Coupling with ice ridges*

In this paper, we exploit the invariance of the system (2.1)–(2.2) under rotations in the $(x, y)$-plane. We define a two-dimensional in-plane strain rate for an arbitrary velocity field $\boldsymbol{v} = (v_1, v_2)$ as

$$D_{ij}(\boldsymbol{v}) = \frac{1}{2}\left(\frac{\partial v_i}{\partial x_j} + \frac{\partial v_j}{\partial x_i}\right) \tag{2.5}$$

with $i$, $j$ ranging over $\{1, 2\}$ (note that $\boldsymbol{v}$ in parentheses here denotes the argument of the linear differential operator $D_{ij}$, not a factor). This allows us to write a depth-integrated viscous stress tensor $T_{ij}(\boldsymbol{u})$ as (see also Morland 1987)

$$T_{ij}(\boldsymbol{u}) = Bh[D_{kl}(\boldsymbol{u})D_{kl}(\boldsymbol{u})/2 + D_{kk}(\boldsymbol{u})^2/2]^{(p-2)/2}[D_{ij}(\boldsymbol{u}) + D_{mm}(\boldsymbol{u})\delta_{ij}], \tag{2.6}$$

where $\delta_{ij}$ is the usual Kronecker delta and the summation convention applies, with subscripts $i, j$ ranging over $\{1, 2\}$. Again, $(\boldsymbol{u})$ denotes the argument of $T_{ij}$, not a factor. Omitting this argument temporarily, (2.1)–(2.2) can be put more succinctly as

$$\frac{\partial T_{ij}}{\partial x_j} + f_i - \tau_c u_i/|\boldsymbol{u}| = 0, \qquad |\boldsymbol{u}| > 0 \tag{2.7}$$

in $\Omega_{\text{stream}}$ and $\Omega_{\text{shelf}}$, where the gravitational driving force $\boldsymbol{f} = (f_1, f_2)$ is given by

$$f_i = -\rho g h \frac{\partial s}{\partial x_i}. \tag{2.8}$$

A simple exercise in substitution will confirm that (2.7) with $T_{ij}$ given by (2.6) does indeed take the form (2.1) with $\nu$ given by (2.3).

The ice in ice ridges, where there is no sliding, flows predominantly in vertical rather than horizontal shear. As the vertical length scale involved – the ice thickness – is small compared with the horizontal distances involved in ice stream and ice shelf flow, ice velocities in ridges are small compared with those in streams and shelves (see also Appendix A). Hence we put at leading order

$$\boldsymbol{u} = \boldsymbol{0}, \qquad T_{ij}(\boldsymbol{u}) = 0, \qquad |\boldsymbol{f}| \leqslant \tau_c \tag{2.9}$$

https://doi.org/10.1017/S0022112006009591 Published online by Cambridge University Press

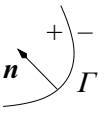



FIGURE 2. Forces on an arc of boundary $\Gamma$.

in $\Omega_{\text{ridge}}$, where the last inequality additionally signifies that the gravitational driving force is supported locally at the bed and must therefore not exceed the yield stress.

It remains to impose jump conditions at the boundaries between ridges, streams and shelves. One obvious condition is that velocities should be continuous across these boundaries, as a finite jump in velocity in our depth-integrated model would correspond to large strain rates in a boundary layer between the different types of flow, large being relative to other parts of the ice sheet. To cause such large strain rates, stresses which are large compared with those acting anywhere else in the ice would be necessary.

A stress jump condition also arises. Let $\Gamma$ be an arc of one of the boundaries between $\Omega_{\text{shelf}}$, $\Omega_{\text{stream}}$ and $\Omega_{\text{ridge}}$ in the $(x, y)$-plane, and choose a definite direction in which this arc is to be traversed. We use superscripts + amd − to indicate limiting values taken as $\Gamma$ is approached from the left and right, respectively (figure 2), and define $\boldsymbol{n}$ as a unit normal to $\Gamma$ pointing to the left. Then the force exerted on that boundary from the left and right can be shown to be (Appendix A, see also MacAyeal 1996, chapter 3)

$$\pm \int_\Gamma T_{ij}^{\pm} n_j - \tfrac{1}{2}\rho g (h^{\pm})^2 n_i / 2 \, \mathrm{d}\Gamma, \tag{2.10}$$

where the '+' and '−' signs are chosen consistently according to whether the force from the left or right is calculated, respectively. Requiring that the total force vanishes then leaves

$$(T_{ij}^{+} - T_{ij}^{-}) n_j = \tfrac{1}{2}\rho g [(h^{+})^2 - (h^{-})^2] \tag{2.11}$$

as $\Gamma$ is arbitrary. (This is effectively a variant of the usual 'pillbox' argument used to demonstrate stress continuity across boundaries in three-dimensional continuum mechanics.) In the remainder of the paper, we shall assume that ice thickness is continuous across the boundaries of streams, shelves and ridges, which then requires that $T_{ij} n_j$ should be continuous across these boundaries.

We should, however, point out that it is unclear whether continuity of ice thickness $h$ is preserved as the ice sheet geometry evolves (a problem which we do not address here, but see also § 5), even if it is true for the initial conditions in a dynamic version of our model. In fact, it cannot be ruled out that real ice streams show some evidence of ice thickness jumps across their margins (Richard Hindmarsh, personal communication, October 2005), in which case the full stress jump conditions (2.11) become necessary.

Lastly, we require boundary conditions at the boundary $\partial\Omega$ of the domain. We assume that this is a calving front, where the ice shelf meets the ocean. Here, an imblance between the hydrostatic forces exerted by the ocean and the shelf requires a non-zero depth-integrated deviatoric stress of the form (cf. Shumskiy & Krass 1976; Morland & Zainuddin 1987)

$$T_{ij} n_j = \frac{1}{2}\left(1 - \frac{\rho}{\rho_w}\right) \rho g h^2 n_i \doteq F_i, \tag{2.12}$$

where $\boldsymbol{n}$ is the outward-pointing normal to $\partial\Omega$ and the last equality defines the boundary force $\boldsymbol{F}$.

https://doi.org/10.1017/S0022112006009591 Published online by Cambridge University Press

## 3. A variational formulation

We suppose that (2.7) holds in $\Omega_{\text{stream}}$ and $\Omega_{\text{shelf}}$ (with $\tau_c = 0$ in the latter), while (2.9) holds in $\Omega_{\text{ridge}}$, and that $\boldsymbol{u}$ and $T_{ij}n_j$ are continuous across the boundaries between these regions. At the calving front $\partial\Omega$, we have the boundary condition (2.12), and we recall that $\partial\Omega$ by assumption does not border either $\Omega_{\text{ridge}}$ or $\Omega_{\text{stream}}$.

The standard way to obtain a variational formulation for the problem at hand is to multiply (2.7) by $u_i - v_i$ and to integrate over the relevant subdomains, assuming these and the integrands involved to be sufficiently smooth to apply the divergence theorem. Here $\boldsymbol{v}$ is a vector test function which is smooth in each subdomain and continuous across the boundaries between the subdomains. Integrating over $\Omega_{\text{stream}}$ then yields

$$\int_{\Omega_{\text{stream}}} \frac{\partial T_{ij}}{\partial x_j}(u_i - v_i) + \boldsymbol{f}\cdot(\boldsymbol{u}-\boldsymbol{v}) - \frac{\tau_c \boldsymbol{u}\cdot(\boldsymbol{u}-\boldsymbol{v})}{|\boldsymbol{u}|}\,\mathrm{d}\Omega = 0, \tag{3.1}$$

and on application of the divergence theorem, we find

$$\int_{\Omega_{\text{stream}}} T_{ij}\frac{\partial(v_i-u_i)}{\partial x_j} + \frac{\tau_c \boldsymbol{u}\cdot(\boldsymbol{v}-\boldsymbol{u})}{|\boldsymbol{u}|} - \boldsymbol{f}\cdot(\boldsymbol{v}-\boldsymbol{u})\,\mathrm{d}\Omega - \int_{\Gamma_{\text{shelf-stream}}} T_{ij}n_j(v_i-u_i)\,\mathrm{d}\Gamma = 0, \tag{3.2}$$

as $T_{ij}n_j = 0$ on $\Gamma_{\text{stream-ridge}}$ by the continuity of $T_{ij}n_j$ across that boundary and because $T_{ij} = 0$ in $\Omega_{\text{ridge}}$. An analogous equation arises for the ice shelf, and adding this to (3.2) leads to a cancellation of the boundary integral over $\Gamma_{\text{shelf-stream}}$:

$$\int_{\Omega_{\text{stream}}\cup\Omega_{\text{shelf}}} T_{ij}\frac{\partial(v_i-u_i)}{\partial x_j} + \frac{\tau_c \boldsymbol{u}\cdot(\boldsymbol{v}-\boldsymbol{u})}{|\boldsymbol{u}|} - \boldsymbol{f}\cdot(\boldsymbol{v}-\boldsymbol{u})\,\mathrm{d}\Omega - \int_{\partial\Omega} \boldsymbol{F}\cdot(\boldsymbol{v}-\boldsymbol{u})\,\mathrm{d}\Gamma = 0, \tag{3.3}$$

where we have defined $\tau_c$ to be zero in $\Omega_{\text{shelf}}$. Since $\tau_c$ is non-negative, we have by Cauchy's inequality that

$$\int_{\Omega_{\text{stream}}\cup\Omega_{\text{shelf}}} \tau_c|\boldsymbol{v}|\,\mathrm{d}\Omega = \int_{\Omega_{\text{stream}}\cup\Omega_{\text{shelf}}} \frac{\tau_c|\boldsymbol{v}||\boldsymbol{u}|}{|\boldsymbol{u}|}\,\mathrm{d}\Omega \geqslant \int_{\Omega_{\text{stream}}\cup\Omega_{\text{shelf}}} \frac{\tau_c \boldsymbol{u}\cdot\boldsymbol{v}}{|\boldsymbol{u}|}\,\mathrm{d}\Omega. \tag{3.4}$$

Using this, and the fact that $T_{ij}$ is symmetric, so $T_{ij}\partial(v_i-u_i)/\partial x_j = T_{ij}D_{ij}(\boldsymbol{v}-\boldsymbol{u})$, we find

$$\int_{\Omega_{\text{stream}}\cup\Omega_{\text{shelf}}} T_{ij}D_{ij}(\boldsymbol{v}-\boldsymbol{u}) + \tau_c(|\boldsymbol{v}|-|\boldsymbol{u}|) - \boldsymbol{f}\cdot(\boldsymbol{v}-\boldsymbol{u})\,\mathrm{d}\Omega - \int_{\partial\Omega} \boldsymbol{F}\cdot(\boldsymbol{v}-\boldsymbol{u})\,\mathrm{d}\Gamma \geqslant 0. \tag{3.5}$$

Moreover, on $\Omega_{\text{ridge}}$, we have $\boldsymbol{u} = \boldsymbol{0}$ and $T_{ij}(\boldsymbol{u}) = 0$, so

$$\int_{\Omega_{\text{ridge}}} T_{ij}D_{ij}(\boldsymbol{v}-\boldsymbol{u})\,\mathrm{d}\Omega + \tau_c(|\boldsymbol{v}|-|\boldsymbol{u}|) - \boldsymbol{f}\cdot(\boldsymbol{v}-\boldsymbol{u})\,\mathrm{d}\Omega$$
$$= \int_{\Omega_{\text{ridge}}} \tau_c|\boldsymbol{v}| - \boldsymbol{f}\cdot\boldsymbol{v}\,\mathrm{d}\Omega \geqslant \int (\tau_c - |\boldsymbol{f}|)|\boldsymbol{v}|\,\mathrm{d}\Omega \geqslant 0. \tag{3.6}$$

Adding the first expression in this inequality to the left-hand side of (3.5), we find that $\boldsymbol{u}$ must satisfy the variational inequality

$$\int_{\Omega} T_{ij}(\boldsymbol{u})D_{ij}(\boldsymbol{v}-\boldsymbol{u}) + \tau_c(|\boldsymbol{v}|-|\boldsymbol{u}|) - \boldsymbol{f}\cdot(\boldsymbol{v}-\boldsymbol{u})\,\mathrm{d}\Omega - \int_{\partial\Omega} \boldsymbol{F}\cdot(\boldsymbol{v}-\boldsymbol{u})\,\mathrm{d}\Gamma \geqslant 0 \tag{3.7}$$

for all sufficiently smooth $\boldsymbol{v}$. The advantage of considering this variational formulation is that it does not contain the different subdomains $\Omega_{\text{shelf}}$, $\Omega_{\text{stream}}$ and $\Omega_{\text{ridge}}$ explicitly,

https://doi.org/10.1017/S0022112006009591 Published online by Cambridge University Press

and when solving the variational inequality (3.7), the free boundaries between ice stream and ice ridge flow need not be tracked explicitly.

Interestingly, solutions of the variational problem (3.7), and hence of the original free boundary problem, are not guaranteed to exist. It is in principle conceivable – though less so in practice for a real ice sheet – that the total applied (gravitational) force is greater than the maximum friction force which the bed is able to generate, or that the total moment of applied forces is greater than the maximum moment which the bed is able to generate. Physically, we expect no solution to exist under these conditions. To see that (3.7) also has no solutions under these circumstances, define $\mathscr{R}$ to be the set of rigid body motions, that is, of velocity fields of the form

$$\boldsymbol{r}(x, y) = (v_1 + \omega y, v_2 - \omega x), \qquad v_1,\ v_2,\ \omega \in \mathbb{R}\ \text{constant}. \tag{3.8}$$

It is straightforward to prove that $D_{ij}(\boldsymbol{r}) = 0$ for any $\boldsymbol{r} \in \mathscr{R}$. Suppose then that for some $\boldsymbol{r}_0 \in \mathscr{R}$ the following inequality holds:

$$\int_\Omega \tau_c |\boldsymbol{r}_0| - \boldsymbol{f} \cdot \boldsymbol{r}_0 \,\mathrm{d}\Omega - \int_{\partial\Omega} \boldsymbol{F} \cdot \boldsymbol{r}_0 \,\mathrm{d}\Gamma < 0. \tag{3.9}$$

By putting $\boldsymbol{v} = \boldsymbol{u} + \boldsymbol{r}_0$ in (3.7) and using $D_{ij}(\boldsymbol{r}_0) = 0$, we obtain

$$\begin{aligned} 0 &\leqslant \int_\Omega T_{ij}(\boldsymbol{u}) D_{ij}(\boldsymbol{r}_0) + \tau_c(|\boldsymbol{u} + \boldsymbol{r}_0| - |\boldsymbol{u}|) - \boldsymbol{f} \cdot \boldsymbol{r}_0 \,\mathrm{d}\Omega - \int_{\partial\Omega} \boldsymbol{F} \cdot \boldsymbol{r}_0 \,\mathrm{d}\Gamma \\ &\leqslant \int_\Omega \tau_c |\boldsymbol{r}_0| - \boldsymbol{f} \cdot \boldsymbol{r}_0 \,\mathrm{d}\Omega - \int_{\partial\Omega} \boldsymbol{F} \cdot \boldsymbol{r}_0 \,\mathrm{d}\Gamma, \end{aligned} \tag{3.10}$$

as a necessary condition for a solution $\boldsymbol{u}$ to exist. This is however a contradiction to (3.9), and hence (3.7) cannot have a solution. If $\boldsymbol{r}_0$ is simply a constant velocity, then (3.9) states that the applied forces are greater than the maximum friction force which the bed can generate. If $\boldsymbol{r}_0$ is of the form (3.8) with $\omega \neq 0$, then we have $\boldsymbol{r}_0 = \omega(y - y_0, x_0 - x)$ for some fixed $(x_0, y_0) \in \mathbb{R}^2$, and (3.9) states that the total moment of applied forces about the point $(x_0, y_0)$ is greater than the maximum moment of frictional forces about $(x_0, y_0)$. This possibility of non-existence of solutions – which also occurs in the unidirectional flow case studied in Schoof (2006) – leads us to investigate the existence of solutions more closely. In addition, we consider in Appendix B under what circumstances solutions for the velocity field $\boldsymbol{u}$ are unique and stable to small perturbations in the 'data functions' $\tau_c$, $\boldsymbol{f}$ and $\boldsymbol{F}$.

### 3.1. *Weak solutions*

In order to apply the powerful apparatus of convex analysis to the problem at hand, we ease the smoothness assumptions imposed on $\boldsymbol{u}$ and $\boldsymbol{v}$. Let $[W^{1,p}(\Omega)]^2$ be the usual Sobolev space endowed with the norm

$$\|\boldsymbol{v}\| = \left[ \int_\Omega (v_i v_i)^{p/2} + \left( \frac{\partial v_i}{\partial x_j} \frac{\partial v_i}{\partial x_j} \right)^{p/2} \mathrm{d}\Omega \right]^{1/p}. \tag{3.11}$$

We consider any $\boldsymbol{u} \in [W^{1,p}(\Omega)]^2$ to be a weak solution of the boundary value problem in the previous section if it satisfies the variational inequality (3.7) for all $\boldsymbol{v} \in [W^{1,p}(\Omega)]^2$. The study of weak solutions is a standard procedure in mathematical analysis (e.g. Evans 1998), motivated by the fact that a classical solution (which has the smoothness properties assumed until now) is also a weak solution (a classical solution satisfies (3.7) and lies in $[W^{1,p}(\Omega)]^2$). By allowing a wider class of functions to be considered as solutions, we simplify the task of proving qualitative attributes of

https://doi.org/10.1017/S0022112006009591 Published online by Cambridge University Press

the problem – for instance, we can study more easily whether it has a solution at all, which, as demonstrated above, need not be the case. Moreover, our uniqueness result also ensures that, if a classical solution solution exists, then all weak solutions are classical solutions, so that the consideration of a wider class of admissible functions then does not introduce any spurious unphysical solutions.

To be definite, we also suppose that $h \in L^{\infty}(\Omega)$ with $h \geqslant h_0 > 0$ almost everywhere, where $h_0$ is a constant. This condition, which ensures ellipticity, requires that ice thickness does not vanish anywhere, and is physically reasonable provided that the ice sheet has no land-based margins. In addition, we assume that $\tau_c \in L^{p/(p-1)}(\Omega)$, $\tau_c \geqslant 0$ almost everywhere, and that $\boldsymbol{f} \in [L^{p/(p-1)}(\Omega)]^2$, $\boldsymbol{F} = [L^{p/(p-1)}(\partial\Omega)]^2$. Lastly, we require $\Omega$ to be open, connected and bounded with a Lipshitzian boundary so that Korn's inequality applies (e.g. Kikuchi & Oden 1988, chapter 5).

Given these assumptions, the results in Evans (1998, pp. 451–452) show that the operator $A$ defined by

$$\langle A\boldsymbol{u}, \boldsymbol{v}\rangle = \int_{\Omega} T_{ij}(\boldsymbol{u}) D_{ij}(\boldsymbol{v})\, \mathrm{d}\Omega \tag{3.12}$$

is the Gâteaux derivative of the convex functional

$$\frac{1}{p}\int_{\Omega} 2Bh[D_{ij}(\boldsymbol{v})D_{ij}(\boldsymbol{v})/2 + D_{ii}(\boldsymbol{v})^2/2]^{p/2}\, \mathrm{d}\Omega,$$

and standard methods of convex analysis (Ekeland & Temam 1976, chapter 2) then show that the solution of the variational inequality (3.7) is equivalent to finding a minimizer $\boldsymbol{u} \in [W^{1,p}(\Omega)]^2$ of the functional $J(\cdot)$ defined by

$$J(\boldsymbol{v}) = \int_{\Omega} \frac{2Bh}{p}[D_{ij}(\boldsymbol{v})D_{ij}(\boldsymbol{v})/2 + D_{ii}(\boldsymbol{v})^2/2]^{p/2} + \tau_c|\boldsymbol{v}| - \boldsymbol{f}\cdot\boldsymbol{v}\, \mathrm{d}\Omega - \int_{\partial\Omega} \boldsymbol{F}\cdot\boldsymbol{v}\, \mathrm{d}\Gamma, \tag{3.13}$$

which is analogous to minimization problems which arise in elastic friction problems (Kikuchi & Oden 1988, chapter 10), though these often involve only the quadratic case $p = 2$.

$J(\cdot)$ is convex, proper and lower semicontinuous on $[W^{1,p}(\Omega)]^2$. The remaining ingredient in demonstrating the existence of solutions is coercivity – meaning that $J(\boldsymbol{v})$ tends to infinity as $\|\boldsymbol{v}\|$ does, so that $J(\cdot)$ is not minimized 'at infinity' in $[W^{1,p}(\Omega)]^2$. As was shown above, the existence of solutions and hence coercivity are not immediately obvious, which can be attributed to the operator $A$ not being coercive (specifically, the strain-rate tensor $D_{ij}(\boldsymbol{v})$ is invariant under addition of rigid body motions, $\boldsymbol{v} \mapsto \boldsymbol{v} + \boldsymbol{r}$, $\boldsymbol{r} \in \mathscr{R}$, and hence we can let $\|\boldsymbol{v}\|$ tend to infinity while keeping $\langle A\boldsymbol{v}, \boldsymbol{v}\rangle$ bounded). However, we can show that a weak solution $\boldsymbol{u}$ must exist if for all $\boldsymbol{r} \in \mathscr{R}$, $\boldsymbol{r} \neq \boldsymbol{0}$, the following strong form of (3.10) holds:

$$\int_{\Omega} \tau_c|\boldsymbol{r}| - \boldsymbol{f}\cdot\boldsymbol{r}\, \mathrm{d}\Omega - \int_{\partial\Omega} \boldsymbol{F}\cdot\boldsymbol{r}\, \mathrm{d}\Omega > 0, \tag{3.14}$$

or equivalently, as $\mathscr{R}$ is finite-dimensional,

$$\int_{\Omega} \tau_c|\boldsymbol{r}| - \boldsymbol{f}\cdot\boldsymbol{r}\, \mathrm{d}\Omega - \int_{\partial\Omega} \boldsymbol{F}\cdot\boldsymbol{r}\, \mathrm{d}\Omega > \delta_{\mathscr{R}}\|\boldsymbol{r}\|, \tag{3.15}$$

for some fixed $\delta_{\mathscr{R}} > 0$ and all $\boldsymbol{r} \in \mathscr{R}$. Physically, this ensures that the total applied force is less than the maximum friction force which the bed can exert, and that the total moment of applied forces is less than the total moment which friction forces can supply.

https://doi.org/10.1017/S0022112006009591 Published online by Cambridge University Press

In order to prove the existence of a solution when (3.15) holds, we follow Duvaut & Lions (1976) and Kikuchi & Oden (1988), and demonstrate that there is an $R_0 > 0$ such that $J(\boldsymbol{v}) > J(\boldsymbol{0}) = 0$ whenever $\|v\| > R_0$. Any minimizer of $J(\cdot)$ over the closed, bounded and convex set $\{\boldsymbol{v} \in [W^{1,p}(\Omega)]^2 : \|v\| \leqslant R_0\}$ then minimizes $J(\cdot)$ over the whole of $[W^{1,p}(\Omega)]^2$, and by standard methods in convex analysis (Ekeland & Temam 1976, chapter 2), such a minimizer must exist.

In order to apply Korn's inequality, take any $\boldsymbol{v} \in [W^{1,p}(\Omega)]^2$ and decompose it into a rigid body motion $\boldsymbol{v}_{\mathscr{R}} \in \mathscr{R}$ and a remainder $\tilde{\boldsymbol{v}}$ as

$$\left.\begin{aligned} &\bar{\boldsymbol{v}} = (\mathrm{meas}(\Omega))^{-1} \int_\Omega \boldsymbol{v}\,\mathrm{d}\Omega, \qquad \omega = (2\mathrm{meas}(\Omega))^{-1} \int_\Omega \frac{\partial v_1}{\partial x_2} - \frac{\partial v_2}{\partial x_1}\,\mathrm{d}\Omega \\ &\boldsymbol{v}_{\mathscr{R}} = \bar{\boldsymbol{v}} + \omega(x_2, -x_1), \qquad \tilde{\boldsymbol{v}} = \boldsymbol{v} - \boldsymbol{v}_{\mathscr{R}}. \end{aligned}\right\} \tag{3.16}$$

Then, using Korn's second inequality (Wang 2003) and (3.15) as well as Hölder's inequality,

$$\begin{aligned} J(\boldsymbol{v}) &\geqslant \frac{2Bh_0}{p} \int_\Omega [D_{ij}(\tilde{\boldsymbol{v}})D_{ij}(\tilde{\boldsymbol{v}})/2 + D_{ii}(\tilde{\boldsymbol{v}})^2/2]^{p/2}\,\mathrm{d}\Omega + \int_\Omega \tau_c|\boldsymbol{v}_{\mathscr{R}}| - \boldsymbol{f}\cdot\boldsymbol{v}_{\mathscr{R}}\,\mathrm{d}\Omega \\ &\quad - \int_{\partial\Omega} \boldsymbol{F}\cdot\boldsymbol{v}_{\mathscr{R}}\,\mathrm{d}\Gamma - \int_\Omega (\tau_c|\tilde{\boldsymbol{v}}| + \boldsymbol{f}\cdot\tilde{\boldsymbol{v}})\,\mathrm{d}\Omega - \int_{\partial\Omega} \boldsymbol{F}\cdot\tilde{\boldsymbol{v}}\,\mathrm{d}\Gamma \\ &\geqslant \frac{2Bh_0C_1}{p}\,\|\tilde{\boldsymbol{v}}\|^p + \delta_{\mathscr{R}}\,\|\boldsymbol{v}_{\mathscr{R}}\| - \big(\|\tau_c\|_{L^{p/(p-1)}(\Omega)} \\ &\quad + \|\boldsymbol{f}\|_{[L^{p/(p-1)}(\Omega)]^2} + C_2\,\|\boldsymbol{F}\|_{[L^{p/(p-1)}(\partial\Omega)]^2}\big)\,\|\tilde{\boldsymbol{v}}\|, \end{aligned} \tag{3.17}$$

where $C_1 > 0$ depends only on $p$ and $\Omega$, and $C_2$ is the norm of the trace operator from $[W^{1,p}(\Omega)]^2$ into $[L^p(\partial\Omega)]^2$. Hence $J(\boldsymbol{v}) \geqslant \alpha(\|\tilde{\boldsymbol{v}}\|^p - \beta\,\|\tilde{\boldsymbol{v}}\| + \gamma\,\|\boldsymbol{v}_{\mathscr{R}}\|)$ for appropriate positive $\alpha$, $\beta$ and $\gamma$. Writing $R = \|\boldsymbol{v}_{\mathscr{R}}\| + \|\tilde{\boldsymbol{v}}\|$ and minimizing $\alpha(\|\tilde{\boldsymbol{v}}\|^p - \beta\,\|\tilde{\boldsymbol{v}}\| + \gamma\,\|\boldsymbol{v}_{\mathscr{R}}\|)$ over $\|\tilde{\boldsymbol{v}}\|$ while keeping $R$ constant, it is straightforward to show that the right-hand side of this inequality is positive provided

$$\|\tilde{\boldsymbol{v}}\| + \|\boldsymbol{v}_{\mathscr{R}}\| \geqslant \|\boldsymbol{v}\| > R_0 = \frac{p-1}{\gamma}\left[\frac{\beta+\gamma}{p}\right]^{p/(p-1)}, \tag{3.18}$$

and the desired result follows.

Having proved that solutions exist under physically plausible circumstances, we naturally want to know whether there can be more than one solution: are the location and flow velocities of ice streams uniquely defined by ice sheet geometry and basal yield stresses? This problem – which is largely left open by Duvaut & Lions (1976) and Kikuchi & Oden (1988) – is somewhat involved because multiple solutions are possible under very specific circumstances. A detailed discussion can be found in Appendix B, while we only summarize our results here. As in Duvaut & Lions (1976) and Kikuchi & Oden (1988), it is relatively straightforward to show that if two distinct solutions $\boldsymbol{u}_1$ and $\boldsymbol{u}_2$ of (3.7) exist, they can differ only by a rigid body velocity $\boldsymbol{r}_\Delta \in \mathscr{R}$. One can then use convexity arguments to demonstrate that both solutions must be such that the velocity vectors $\boldsymbol{u}_1$ and $\boldsymbol{u}_2$ are parallel to $\boldsymbol{r}_\Delta$ in regions where the yield stress $\tau_c$ is non-zero. Moreover, as we show in Appendix B (where we also discuss the stability of solutions to perturbations in the data functions), the regions where $\boldsymbol{u}_1$ (or $\boldsymbol{u}_2$) points in the same direction as $\boldsymbol{r}_\Delta$ and those in which it is oriented opposite to $\boldsymbol{r}_\Delta$ must satisfy a certain integral equation. We note that these conditions for non-uniqueness will be satisfied by a solution $\boldsymbol{u}$ only for very special

https://doi.org/10.1017/S0022112006009591 Published online by Cambridge University Press

combinations of the functions $h$, $\tau_c$, $\boldsymbol{f}$ and $\boldsymbol{F}$, and in almost all cases, we can expect solutions to be unique. In addition, if $\boldsymbol{u}_1$ and $\boldsymbol{u}_2 = \boldsymbol{u}_1 + \boldsymbol{r}_\Delta$ are distinct solutions, then, by the convexity of $J(\cdot)$, $\boldsymbol{u}_\lambda = \boldsymbol{u}_1 + \lambda \boldsymbol{r}_\Delta$ is also a solution for $\lambda \in (0, 1)$. It can be shown that for any $\lambda$ in that range, $\boldsymbol{u}_\lambda$ is such that sliding occurs almost everywhere in the region where $\tau_c$ is non-zero (see Appendix B). In other words, if there are two solutions, then they are connected by a family of solutions in which sliding occurs everywhere in the region where the basal yield stress is non-zero. The existence of such solutions is an unlikely prospect for a real ice sheet, and in general, we expect solutions to be unique for realistic ice sheets.

## 4. Numerical results

One of the main advantages of the variational formulation developed above is that it leads directly to a numerical method for solving the ice flow problem, based on looking for a minimzer of the functional (3.13). The main challenge here is to deal with the non-differentiability of the friction functional $\int_\Omega \tau_c |\boldsymbol{v}| \, \mathrm{d}\Omega$. To avoid this issue, we consider a sequence of regularized problems in which we consider the minimization of functionals of the form

$$J_\epsilon(\boldsymbol{v}) = \int_\Omega \frac{2Bh}{p} [\epsilon^2/L^2 + D_{ij}(\boldsymbol{v}) D_{ij}(\boldsymbol{v})/2 + D_{ii}(\boldsymbol{v})^2/2]^{p/2} \, \mathrm{d}\Omega + \int_\Omega \tau_c \sqrt{\epsilon^2 + |\boldsymbol{v}|^2} - \boldsymbol{f} \cdot \boldsymbol{v} \, \mathrm{d}\Omega - \int_{\partial\Omega} \boldsymbol{F} \cdot \boldsymbol{v} \, \mathrm{d}\Gamma, \quad (4.1)$$

letting the parameter $\epsilon$ tend to zero, where $L$ is a fixed length scale characteristic of the problem (required here for dimensional reasons, as $\epsilon$ represents a velocity). The functionals $J_\epsilon(\cdot)$ are then discretized using piecewise-linear finite elements, and the resulting minimization problems are straightforward to solve numerically using a Newton-type method (e.g. Dennis & Schnabel 1996). The use of regularized friction functionals in coercive elastic friction problems was discussed by Kikuchi & Oden (1988, §10.4), and a combination of their results and the techniques used in Appendix B, §B 2 can be used to show that, in the limit $\epsilon \to 0$, minimizers of $J_\epsilon(\cdot)$ (in which we have also regularized viscosity for the case of zero strain rate) tend to the minimizer of $J(\cdot)$, provided the latter is unique.

Exact solutions can be obtained for the special case of an infinite ice slab of uniform thickness $h_0$ inclined at a constant surface slope $\tan\theta$ to the horizontal, provided $\tau_c$ is independent of the downslope coordinate ($x$, say), while it is periodic in the cross-slope coordinate ($y$). Although this differs slightly from the finite ice sheet fringed by ice shelves discussed above, our variational formulation can be adapted easily to this case. In what follows, we put $p = 4/3$, corresponding to the widely used value $n = 3$ in Glen's law (Paterson 1994, chapter 5). We also put $\boldsymbol{f} = (f, 0)$ with $f = \rho g h_0 \tan\theta$, and consider the special case of a yield stress distribution given by $\tau_c = f|y/L|^m$ extended periodically outside the domain $-3L < y < 3L$, where $L$ and $m$ are positive constants. The reason for this choice is purely that it leads to an analytical solution. Defining $W$ to be the half-width of the ice stream, so $y = W$ defines the stream–ridge boundary $\Gamma_{\text{stream-ridge}}$, our model reduces to $\boldsymbol{u} = (u, 0)$ with $u$ and $W$ determined by

$$-\frac{\mathrm{d}}{\mathrm{d}y}\left(\frac{Bh_0}{2}\left|\frac{1}{2}\frac{\mathrm{d}u}{\mathrm{d}y}\right|^{-2/3}\frac{\mathrm{d}u}{\mathrm{d}y}\right) = f(1 - |y/L|^m), \qquad u(\pm W) = \left.\frac{\mathrm{d}u}{\mathrm{d}y}\right|_{y=\pm W} = 0 \quad (4.2)$$

https://doi.org/10.1017/S0022112006009591 Published online by Cambridge University Press

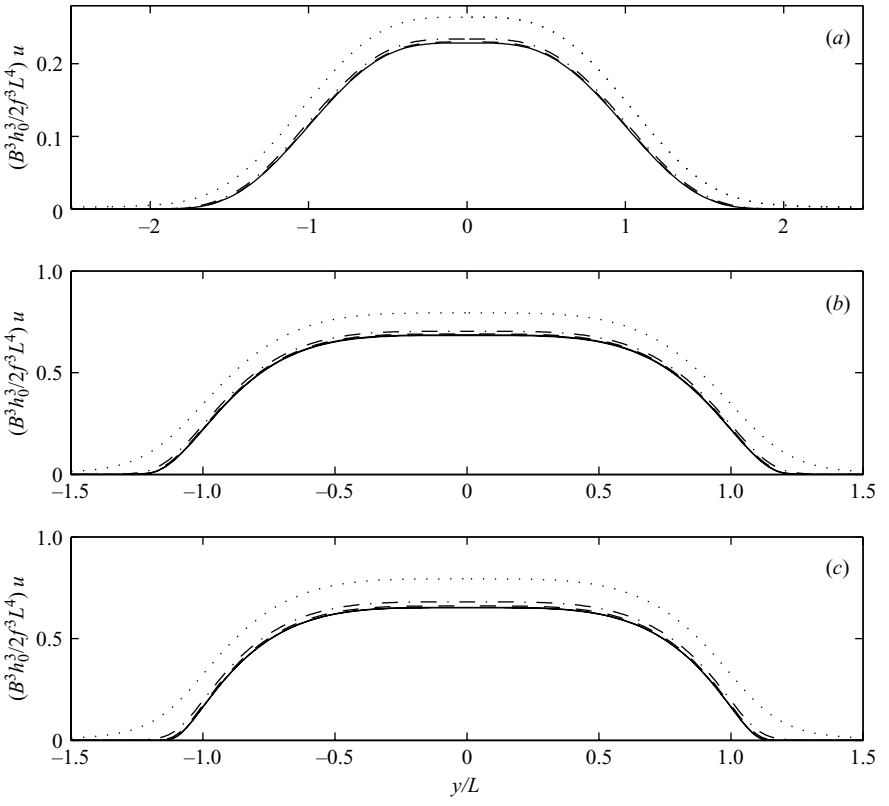



FIGURE 3. Numerical solutions of the depth-integrated ice flow problem compared with analytical solutions and solutions of the full Stokes equations. Each panel shows a numerical solution of the variational problem corresponding to (4.2) as a solid line, with the analytical solution (4.3) also plotted as a solid line. $m$ takes the values 1 ($a$), 10 ($b$) and 20 ($c$). Also plotted in each panel are the corresponding solutions for the full Stokes equations, with depth-to-width ratios $h_0/L$ given by 0.05 (dashed line), 0.1 (dot-dashed line) and 0.25 (dotted line).

in $|y|<W$, $u=0$ elsewhere in $|y|<3L$. The solution is $W=(m+1)^{1/m}L\,(<3L)$, and

$$u=-\frac{2f^3L^4}{B^3h_0^3}\left[\frac{(y/L)^4-(m+1)^{4/m}}{4}-\frac{3\left(|y/L|^{m+4}-(m+1)^{1+4/m}\right)}{(m+1)(m+4)}\right.$$
$$\left.+\frac{3\left(|y/L|^{2m+4}-(m+1)^{2+4/m}\right)}{(m+1)^2(2m+4)}-\frac{|y/L|^{3m+4}-(m+1)^{3+4/m}}{(m+1)^3(3m+4)}\right] \tag{4.3}$$

for $|y|<W$, $u=0$ otherwise in $|y|<3L$. Figure 3 shows numerical solutions plotted against this exact solution for a variety of values of $m$. The two are indistinguishable.

In figure 3, we also compare these results to solutions of the full Stokes equations for the same geometrical set-up, which are calculated using the method in Schoof (2006). Plotted alongside the solutions (4.3) are surface velocity predicted by Schoof (2006) for the same geometry and yield stress function $\tau_c$ for a variety of aspect ratios $h_0/L$, where we have applied periodic boundary conditions at $y=\pm 3L$. The results obtained from the two different methods agree closely for values of $h_0/L$ less than about 0.1, while agreement becomes poorer for larger aspect ratios. Interestingly, this remains true for large values of $m$, in which case the yield stress $\tau_c$ increases sharply

https://doi.org/10.1017/S0022112006009591 Published online by Cambridge University Press

within the boundary layer between ridge and stream flow. Hence sharp gradients in friction appear to be a less serious limitation on our depth-integrated approach than insufficiently small aspect ratios.

### 4.1. *Ice shelf buttressing of ice streams with plastic beds*

A problem which has received considerable attention in glaciology recently is the effect of an ice shelf on the flow of the ice steams which serve as its tributaries. It has been observed that the collapse of an ice shelf can cause the ice streams feeding it to speed up (Rignot *et al.* 2004), and this effect has been attributed to the way in which an ice shelf transmits the boundary force $\boldsymbol{F}$ acting at the calving front to the ice streams behind it (see also MacAyeal 1987); the somewhat misleading term 'backpressure' is often used in glaciology to describe this phenomenon (Paterson 1994, chapter 12). Theoretical studies have generally been limited to ice shelves confined to embayments and fed by ice streams of fixed spatial extent (e.g. MacAyeal 1989; Schmeltz *et al.* 2002). Below, we illustrate the use of our numerical method by considering the effect of removing an ice shelf from a coastline with an alternating pattern of ice ridges and ice streams, whose location is determined by the yield stress of the bed.

Figure 4 shows the ice sheet and ice shelf geometry as well as the basal yield stress distributions used in our calculations. We assume that $h$ and $s$ depend only on the $y$-coordinate while $\tau_c$ depends on $x$ and $y$, and extend our domain periodically in the $x$-direction with period 100 km. The grounding line of the ice sheet is located at $y = 0$, and we consider variable ice shelf extents below $y = 0$. The ice sheet geometry and basal yield stress distribution are are also taken to be symmetrical about $y = 250\,\mathrm{km}$. This allows us to impose the boundary conditions $v = 0$ and $\partial u/\partial y = 0$ at $y = 250\,\mathrm{km}$ by symmetry (assuming a unique solution). Furthermore, we have used the values $p = 4/3$, $B = 3.7 \times 10^8\,\mathrm{Pa\,s^{1/3}}$, $g = 10\,\mathrm{m\,s^{-2}}$, $\rho = 900\,\mathrm{kg\,m^{-3}}$, $\rho_w = 1000\,\mathrm{kg\,m^{-3}}$.

The two yield stress distributions shown in figure 4 represent two possible scenarios: a distribution '*a*' (panel *a*) in which variations in basal yield stress are comparable in size to the driving stress and occur over relatively long distances, and a distribution '*b*' (panel *b*) in which there are strong variations in basal yield stress occurring over relatively short distances. Results for distribution *a* are shown in figure 5(*a*). The presence of an ice shelf has a significant effect on the ice velocities of the grounded part of the ice sheet: In panel (*a*)(*i*), where there is no ice shelf present, ice velocities increase rapidly near the grounding line as one moves in the downstream direction, reaching a maximum of $2200\,\mathrm{m\,a^{-1}}$ (metres per year). In a dynamic model, this would lead to rapid thinning of the ice near the grounding line, and hence a retreat in the position of the grounding line. In panels (*a*)(ii) and (*a*)(iii), the increase in velocities near the grounding line is much less marked, and maximum ice flow velocities are more modest, even within the ice shelf (around $1500\,\mathrm{m\,a^{-1}}$). Interestingly, the spatial extent of streaming flow is slightly greater in panels (*a*)(ii) and (*a*)(iii) than in panel (*a*)(i), especially near the grounding line. The ice shelf transfers part of the boundary force $\boldsymbol{F}$ acting at the calving front away from the ice stream and towards the ice ridges, which causes the ice stream to flow more slowly than it would in the absence of the ice shelf, and which also mobilizes part of the ice ridges.

Results for the yield stress distribution *b* are shown in figure 5(*b*). The effect of removing the ice shelf on ice flow velocities in the stream are similar to those observed for yield stress distribution *a*: the ice stream speeds up considerably when the ice shelf is removed, presumably for the same reasons as before. In addition (though this is difficult to discern visually), there is now less effect on the spatial distribution of streaming flow than for yield stress distribution *a* as a result of the much higher

https://doi.org/10.1017/S0022112006009591 Published online by Cambridge University Press

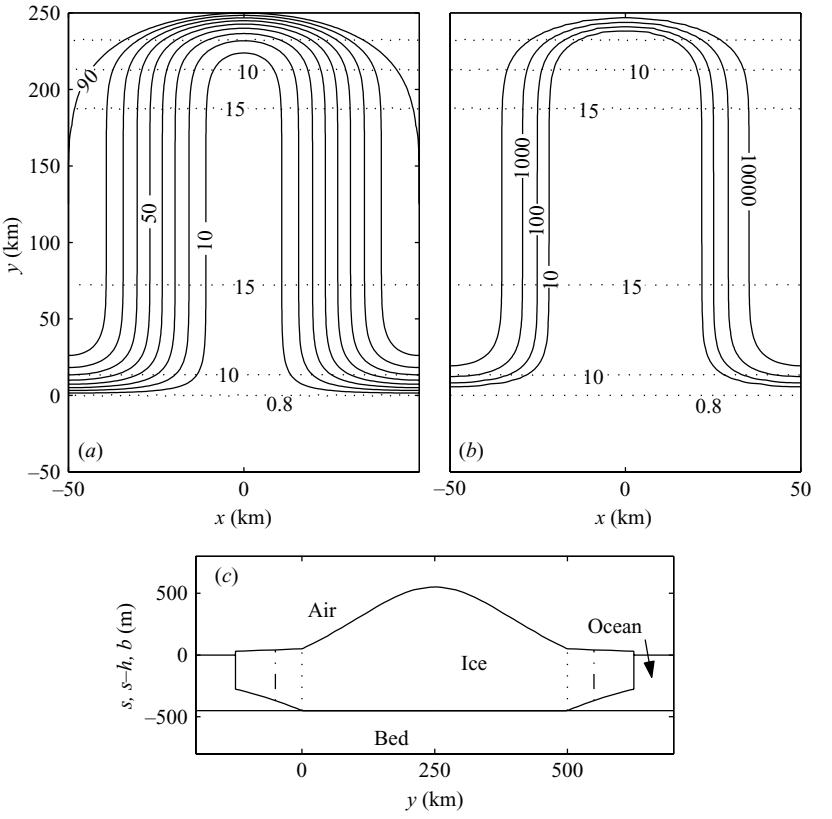



FIGURE 4. Ice sheet geometry and yield stress distributions used in numerical calculations. Panels (*a*) and (*b*) shows contours of basal yield stress distributions '*a*' and '*b*' as solid lines, and contour lines of driving stress $|\boldsymbol{f}|$ as dotted lines. Units are kPa. The ice flow domain extends symmetrically above $y = 250$ km. The domain is also extended periodically in $x$, with period 100 km. The ice surface geometry is shown in (*c*) as a profile along the $y$-axis. Solid lines show the extent of ice, the bed and ocean surface corresponding to the largest ice shelf used (corresponding to (*a*)(iii) and (*b*)(iii) in figure 5). Dotted and dot-dashed lines show the calving front position for the ice sheet geometries corresponding to (*a*)(i), (*b*)(i) and (*a*)(ii), (*b*)(ii) in figure 5, respectively.

basal yield stresses at the bed in the ice ridges, which prevent streaming flow from encroaching on the ice ridges under changes in boundary forcing.

## 5. Discussion

We have so far focused only on the 'diagnostic' problem of determining the regions of streaming flow $\Omega_{\text{stream}}$ and the velocity field $\boldsymbol{u}$ for a given set of yield stresses $\tau_c$ and gravitational forces $\boldsymbol{f}$ and $\boldsymbol{F}$. A dynamic evolution of the ice surface based on the continuity equation

$$\frac{\partial h}{\partial t} + \frac{\partial (h u_i)}{\partial x_i} = a \tag{5.1}$$

may be possible, where $t$ is time and $a$ an ice accumulation rate. It is, however, not immediately obvious whether the ice thickness continuity conditions across ridge–stream boundaries assumed in § 2 would be preserved as $h$ evolves, as the divergence of ice flux $\boldsymbol{u}h$ can be discontinuous across $\Gamma_{\text{stream–ridge}}$. That said, the location of

https://doi.org/10.1017/S0022112006009591 Published online by Cambridge University Press

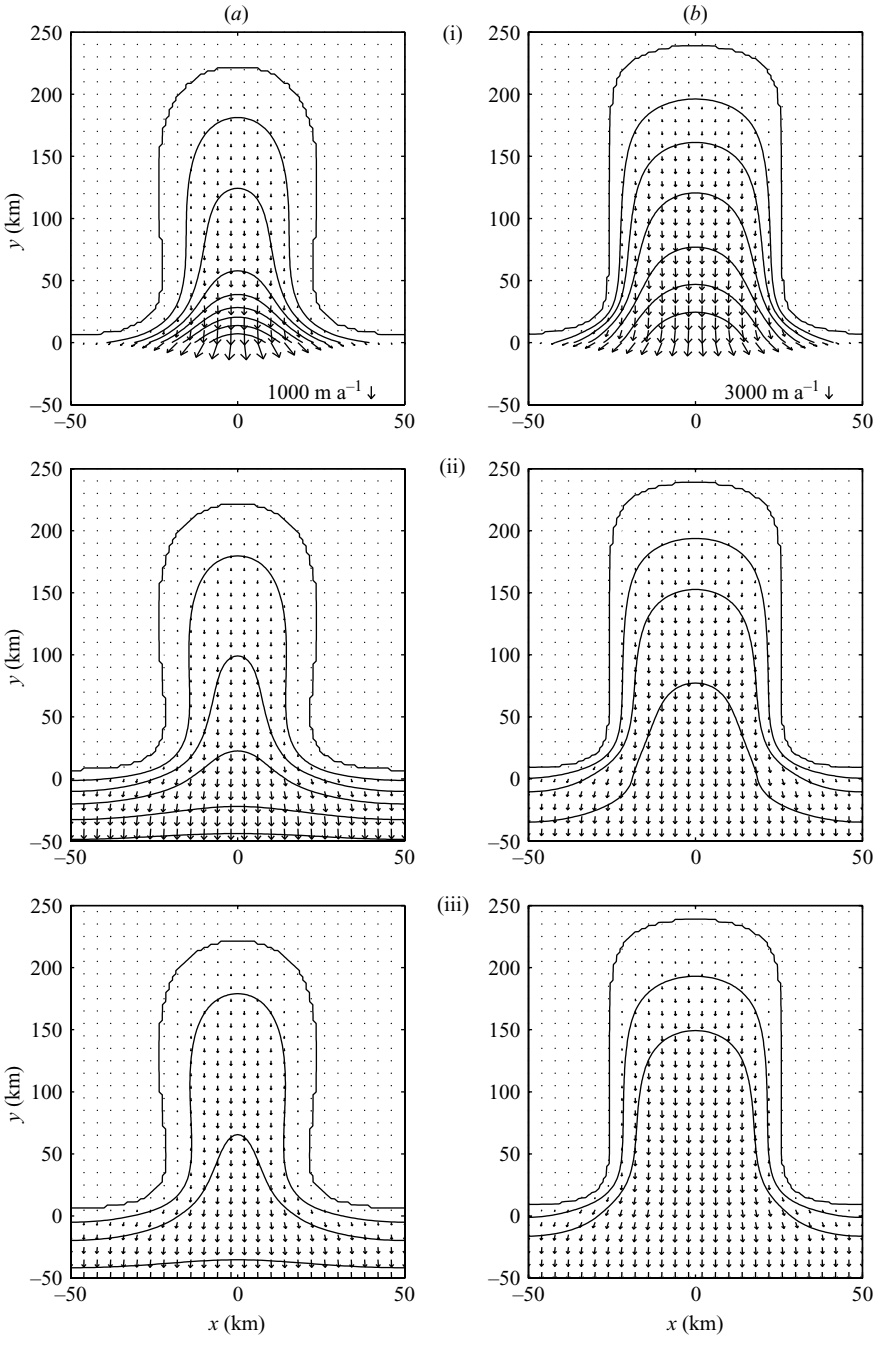



FIGURE 5. Numerical results for the ice sheet geometry and basal yield stress distributions shown in figure 4. Shown are 'quiver' plots of velocity vectors and contours of ice speed $|\boldsymbol{u}|$. Scales for velocity vectors are shown in row (i). Contour intervals are 250 m a$^{-1}$ (metres per year) in column (*a*), and 1250 m a$^{-1}$ in column (*b*). The highest-positioned contour line in each panel corresponds to $\Gamma_{\text{stream-ridge}}$, while $y = 0$ marks the grounding line. The calving front is at $y = 0$ in row (i), at $y = -50$ km in (ii), and at $y = -125$ km in (iii) (for which only part of the shelf is displayed).

https://doi.org/10.1017/S0022112006009591 Published online by Cambridge University Press

the ridge–stream boundary will itself evolve as a result of ice thickness changes, driven by the steepening of the surface as an ice stream drains, which is likely to cause the stream to encroach on its surrounding ice ridges. Whether this is sufficient to prevent discontinuities in ice thickness from evolving at stream–ridge boundaries (which could be considered as an extreme case of a steepened surface) needs to be addressed by future theoretical work. Should ice thickness discontinuities evolve, then our derivation of the stress continuity condition in § 2.2 no longer holds, and the ice flow problem considered in this paper needs to be amended accordingly. In particular, if there is an ice thickness discontinuity with a corresponding ice surface discontinuity, we may expect that the driving force $f_i = \rho g h \partial s/\partial x_i$ will no longer be integrable, in the sense that discontinuous $s$ gives rise to a non-integrable distributional derivative $\partial s/\partial x_i$. How the weak formulation in this paper can be adapted to this case is unclear. For example, it is not feasible to apply the jump condition (2.11) directly unless the location of the stream–ridge boundary is known *a priori*, whereas the point of the weak formulation employed here is that it makes no explicit reference to the location of this free boundary.

Even assuming that the dynamical version of the model is self-consistent and thickness discontinuities do not evolve over time, setting $\boldsymbol{u} = \boldsymbol{0}$ in the ice ridges remains problematic from a practical perspective as it precludes the ice in ice ridges from flowing, and if $a > 0$, the ice there can only thicken continually until ice streams encroach on them. This is not the most useful glaciological scenario: more realistically, a model should account for the slow lubrication flow in ice ridges and for the mass flux that this causes from ice ridges into ice streams. As ice streams are usually long and narrow, this contribution to ice stream flux can be significant even if ridge fluxes are small, in much the same way as slow overland and groundwater flow in a river catchment ultimately control the much faster flow of the river itself. This suggests that our model may be successful at capturing the mechanics of ice streams – in the sense that it gives a correct leading-order determination of the location and flow velocities of streaming flow – but it may not be capable of representing their dynamics adequately as it cannot account for the slow mass transfer across the margins of a long and narrow ice stream.

A possible means of avoiding the zero-velocity boundary condition at the stream–ridge boundary is to use so-called 'first-order models' (Blatter 1995; Colinge & Blatter 1998; Picasso *et al.* 2004) for glacier and ice sheets. These incorporate both vertical shearing and longitudinal and lateral stresses into a single ice flow model which applies to both lubrication-flow-type ice ridges and membrane-type ice streams. This avoids the difficulty associated with having zero depth-integrated velocity at the ridge-stream boundary. Moreover, as we will detail in a separate paper, this type of model, with a Coulomb friction law at the bed, is amenable to a variational treatment analogous to that above. However, among the less attractive features of these first-order models are the fact that they rely on the selective inclusion of higher-order terms in an asymptotic expansion in order to ensure validity under different sliding regimes, and that their behaviour in transition zones between these regimes may be different from the full Stokes equations. Additionally, first-order models are computationally more expensive as the vertical $x_3$-coordinate features explicitly.

## 6. Conclusions

In this paper, we have considered how the spatial extent of ice stream flow within an ice sheet can be determined from a knowledge of the geometry of the ice sheet

https://doi.org/10.1017/S0022112006009591 Published online by Cambridge University Press

and of the spatial distribution of bed yield stresses. Our method is based on widely used depth-integrated models for the flow of ice ridges, ice streams and ice shelves, which allow us to derive a variational characterization of the free boundary between ice streams and ice ridges. As discussed above, the use of depth-integrated models in conjunction with a variational approach is somewhat limited with respect to developing a dynamical description for coupled ice ridge–ice stream flow, insofar as we are forced to assume that ice ridge fluxes are insignificant. Higher-order ice flow models may provide a useful means of avoiding this difficulty. An additional feature which a realistic, dynamic model needs to include is the evolution in time of basal water pressure $p_w(x_1, x_2)$, which presumably controls the spatial patterning of ice streams (see e.g. Fowler & Johnson 1996) and their observed temporal variability (Retzlaff & Bentley 1993; van der Veen & Whillans 1996; Tulaczyk, Kamb & Engelhardt 2000).

As a specific example to which our method can be applied directly, we have studied the effect of ice shelves on the flow velocities and spatial extent of ice stream flow for a given basal yield stress distribution. In line with previous studies, which have concentrated on ice shelves confined to embayments rather than on ice shelves backed by a periodic array of ice streams and ice ridges as we have done, we have found that flow velocities in an ice stream increase markedly when the ice shelf into which an ice stream drains is removed, and this effect can be attributed to the way in which an ice shelf transmits the boundary force $\boldsymbol{F}$ acting at the calving front to the ice ridges and ice shelves upstream of the grounding line. When an ice shelf is present, a greater proportion of this boundary force is transmitted to the ice ridges than in the absence of the ice shelf, thus causing slower ice flow velocities in the ice stream. The same effect can also lead to parts of the ice ridges near the grounding line becoming 'mobilized' and turning into areas of streaming flow when an ice shelf is present compared with the case when there is no ice shelf. The extent to which this effect – which represents the role of ice shelves in moderating the spatial extent of streaming flow – is observed depends on the spatial distribution of yield stresses at the bed. Specifically, this effect is inhibited when yield stresses under ice ridges are high.

In closing, it is worth pointing out that our variational approach is not limited to a pure power-law rheology. Our work above was based on a constitutive relationship for ice of the form $\tau_{ij} = Bd^{p-2}d_{ij}$, where $\tau_{ij}$ is deviatoric stress, $d_{ij}$ is strain rate and $d = (d_{ij}d_{ij}/2)^{1/2}$ its second invariant. However, recent work by Goldsby & Kohlstedt (2001) has suggested that a more complex combination of power laws may be a more appropriate description of ice rheology. In principle, our method can cope with such alternative rheologies of the form $\tau_{ij} = \eta(d^2)d_{ij}$, provided the function $\eta$ is the first derivative of a function $\chi$ which satisfies coercivity and growth constraints of the form $K_1 d^p < \chi(d^2) < K_2(1 + d^p)$ for some $K_1,\ K_2 > 0$, and which is such that $\chi(d^2)$ is convex in $d$. In that case, our method reduces to the minimization of the generalized functional

$$J(\boldsymbol{v}) = \int_\Omega \chi(D_{ij}(\boldsymbol{v})D_{ij}(\boldsymbol{v})/2 + D_{ii}(\boldsymbol{v})^2/2) + \tau_c|\boldsymbol{v}| - \boldsymbol{f}\cdot\boldsymbol{v}\,\mathrm{d}\Omega - \int_{\partial\Omega} \boldsymbol{F}\cdot\boldsymbol{v}\,\mathrm{d}\Gamma. \qquad (6.1)$$

I would like to thank the editor, William Young, as well as Richard Hindmarsh and two anonymous referees, for their scrutiny and constructive criticism. This material is based on work supported by the US National Science Foundation under Grant No. DMS-03227943. Additional funding was provided by a Killam postdoctoral research fellowship at the University of British Columbia.

https://doi.org/10.1017/S0022112006009591 Published online by Cambridge University Press

## Appendix A. Ice stream and ice ridge models

A full three-dimensional model for the incompressible Stokes' flow of the grounded part of the ice sheet is the following. In $b < z < s$, we have the following relations for momentum and mass conservation:

$$\frac{\partial \tau_{ij}}{\partial x_j} - \frac{\partial P}{\partial x_i} - \rho g \delta_{i3} = 0, \qquad \frac{\partial u_i}{\partial x_i} = 0, \tag{A 1}$$

where $P$ (distinct from the rheological exponent $p$) is pressure, and subscripts now range over $\{1, 2, 3\}$. The deviatoric stress $\tau_{ij}$ is defined in terms of the velocity field $\boldsymbol{u} = (u, v, w) = (u_1, u_2, u_3)$ through

$$d_{ij} = \frac{1}{2}\left(\frac{\partial u_i}{\partial x_j} + \frac{\partial u_j}{\partial x_i}\right), \qquad d = \sqrt{d_{ij} d_{ij}/2}, \qquad \tau_{ij} = B d^{p-2} d_{ij}. \tag{A 2}$$

At the surface $z = s$, we have zero applied traction. Defining the normal to the upper surface to be $\boldsymbol{n}_{(s)}$, this becomes

$$\tau_{ij} n_{(s)j} - P n_{(s)i} = 0, \qquad \boldsymbol{n}_{(s)} = \frac{1}{\sqrt{1 + (\partial s/\partial x)^2 + (\partial s/\partial y)^2}}\left(-\frac{\partial s}{\partial x}, -\frac{\partial s}{\partial y}, 1\right). \tag{A 3}$$

At the bed $z = b = s - h$, we have normal vector $\boldsymbol{n}_{(b)}$, compressive normal stress $\sigma_{nn}$ and shear stress $\tau_{(b)i}$ defined by

$$\left.\begin{aligned} \boldsymbol{n}_{(b)} &= \frac{1}{\sqrt{1 + (\partial b/\partial x)^2 + (\partial b/\partial y)^2}}\left(-\frac{\partial b}{\partial x}, -\frac{\partial b}{\partial y}, 1\right), \\ \sigma_{nn} &= P - \tau_{ij} n_{(b)i} n_{(b)j}, \qquad \tau_{(b)i} = \tau_{ij} n_{(b)j} - \tau_{jk} n_{(b)j} n_{(b)k} n_{(b)i}, \end{aligned}\right\} \tag{A 4}$$

and in terms of $\sigma_{nn}$ and water pressure $p_w$, the yield strength of the bed is

$$\tau_c = \mu(\sigma_{nn} - p_w). \tag{A 5}$$

Two possibilities arise: either sliding occurs and the yield stress is attained, so on $z = b$,

$$\tau_{(b)i} = \tau_c u_i/|\boldsymbol{u}| \qquad \text{and} \qquad |\boldsymbol{u}| > 0, \tag{A 6}$$

in which case we also have no normal velocity,

$$u_i n_{(b)i} = 0. \tag{A 7}$$

Alternatively, there is no sliding and basal shear stress is at or below the yield stress

$$\boldsymbol{u} = \boldsymbol{0} \qquad \text{and} \qquad \tau_{(b)i}\tau_{(b)i} \leqslant \tau_c^2. \tag{A 8}$$

### A.1. *Sliding: ice streams*

We first consider the case of sliding, or ice stream flow. Let the region in which sliding occurs have a characteristic horizontal extent $[x]$, which can typically be identified with ice stream width. We suppose $[x]$ is large compared with the typical ice thickness $[h]$, and consider the problem at leading order in the aspect ratio parameter $\epsilon = [h]/[x]$ (naturally, the expansion which results is only applicable away from the boundaries of the ice stream; close to these boundaries a boundary layer exists which matches the ice stream velocity field to that in the surrounding ice ridges). In addition, we let $[s]$ be a scale for variations in surface elevation over distances $[x]$. We assume that surface elevation variations are similar to or less than ice thickness over distances $[x]$, which is appropriate for ice sheets but not for steep valley glaciers, and hence that $\delta = [s]/[h] \lesssim 1$.

https://doi.org/10.1017/S0022112006009591 Published online by Cambridge University Press

Appropriate scales for stresses $[\tau]$ and velocities $[u]$ are then

$$[\tau] = \rho g[s], \qquad [u] = B^{-1/(p-1)}[\tau]^{1/(p-1)}[x]. \tag{A 9}$$

We non-dimensionalize as follows:

$$\left.\begin{aligned} &(x, y, z) = [x](x^*, y^*, \epsilon z^*), \quad h = [h]h^*, \quad s = [s]s^*, \quad (u, v, w) = [u](u^*, v^*, \epsilon w^*), \\ &d = [u][x]^{-1}d^*, \quad (\tau_{11}, \tau_{12}, \tau_{22}, \tau_{13}, \tau_{23}, \tau_{33}) = [\tau](\tau_{11}^*, \tau_{12}^*, \tau_{22}^*, \epsilon\tau_{13}^*, \epsilon\tau_{23}^*, \tau_{33}^*), \\ &P = [\tau]P^* + \rho g(s - z), \quad p_w = \rho g[h]p_w^* \end{aligned}\right\} \tag{A 10}$$

For simplicity, the asterisks on the dimensionless variables are dropped immediately. To the error in $\epsilon$ indicated, we obtain on $\delta s - h < z < \delta s$

$$\frac{\partial \tau_{11}}{\partial x} + \frac{\partial \tau_{12}}{\partial y} + \frac{\partial \tau_{13}}{\partial z} - \frac{\partial P}{\partial x} - \frac{\partial s}{\partial x} = 0, \tag{A 11}$$

$$\frac{\partial(\tau_{33} - P)}{\partial z} = O(\epsilon^2), \tag{A 12}$$

$$\frac{\partial u}{\partial x} + \frac{\partial v}{\partial y} + \frac{\partial w}{\partial z} = 0, \tag{A 13}$$

$$\frac{\partial u}{\partial z} = O(\epsilon^2), \qquad \frac{\partial v}{\partial z} = O(\epsilon^2), \tag{A 14}$$

$$\left.\begin{aligned} &\tau_{11} = d^{p-2}\frac{\partial u}{\partial x}, \qquad \tau_{22} = d^{p-2}\frac{\partial v}{\partial y}, \qquad \tau_{12} = \tau_{21} = \frac{1}{2}d^{p-2}\left(\frac{\partial u}{\partial y} + \frac{\partial v}{\partial x}\right), \\ &\tau_{33} = -\tau_{11} - \tau_{22}. \end{aligned}\right\} \tag{A 15}$$

$$d = \sqrt{\left(\frac{\partial u}{\partial x}\right)^2 + \left(\frac{\partial v}{\partial y}\right)^2 + \frac{\partial u}{\partial x}\frac{\partial v}{\partial y} + \frac{1}{4}\left(\frac{\partial u}{\partial y} + \frac{\partial v}{\partial x}\right)^2} + O(\epsilon^2), \tag{A 16}$$

where we have omitted a number of equations which can be obtained from the above by simply interchanging coordinates $x$ and $y$, velocities $u$ and $v$, and subscripts 1 and 2. At the surface $z = \delta s$,

$$\tau_{13} - \delta\frac{\partial s}{\partial y}\tau_{12} - \delta\frac{\partial s}{\partial x}\tau_{11} + \delta\frac{\partial s}{\partial x}\tau_{33} = 0, \tag{A 17}$$

$$\tau_{33} - P = O(\epsilon^2), \tag{A 18}$$

while at the bed $z = \delta s - h$,

$$\tau_{13} - \frac{\partial(\delta s - h)}{\partial y}\tau_{12} - \frac{\partial(\delta s - h)}{\partial x}\tau_{11} + \frac{\partial(\delta s - h)}{\partial x}\tau_{33} = \mu\epsilon^{-1}[(P - \tau_{33}) + \delta^{-1}(h - p_w)]u/\sqrt{u^2 + v^2} + O(\epsilon), \tag{A 19}$$

where again there are analogues of (A 17) and (A 19) with $x$ and $y$, $u$ and $v$, and subscripts 1 and 2 interchanged. We see that, in order for the right-hand side of (A 19) to be of $O(1)$ when $\mu$ is of $O(1)$, we require that $h - p_w = O(\delta\epsilon)$, that is, water pressure needs to be within $O([s]/[x])$ of overburden. This is borne out by field observations of real ice streams, which confirm the presence of high-pressure water at the bed (Engelhardt & Kamb 1997).

https://doi.org/10.1017/S0022112006009591 Published online by Cambridge University Press

Equation (A 14) justifies the assertion that $u$ and $v$ are independent of depth at leading order, and hence so are $\tau_{11}$, $\tau_{12}$, $\tau_{22}$ and $\tau_{33}$. From (A 12), (A 18) and (A 15), we find at leading order

$$P = \tau_{33} = -\tau_{11} - \tau_{22}. \tag{A 20}$$

Integrating (A 11) over $\delta s - h < z < \delta s$ and using (A 17) and (A 19), we find

$$\frac{\partial}{\partial x}\int_{\delta s-h}^{\delta s}\tau_{11}\,\mathrm{d}z+\frac{\partial}{\partial y}\int_{\delta s-h}^{\delta s}\tau_{12}\,\mathrm{d}z-\frac{\partial}{\partial x}\int_{\delta s-h}^{\delta s}P\,\mathrm{d}z-h\frac{\partial s}{\partial x}-\mu\epsilon^{-1}\delta^{-1}(h-p_w)u/\sqrt{u^2+v^2}=0, \tag{A 21}$$

and combining this with (A 20) and the fact that $\tau_{11}$, $\tau_{12}$ and $\tau_{22}$ are independent of depth, gives

$$\frac{\partial(2h\tau_{11}+h\tau_{22})}{\partial x}+\frac{\partial(h\tau_{12})}{\partial y}-h\frac{\partial s}{\partial x}-\mu\epsilon^{-1}\delta^{-1}(h-p_w)u/\sqrt{u^2+v^2}=0. \tag{A 22}$$

On re-dimensionalizing this equation and using (A 15), we obtain (2.1), and an analogous equation arises from interchanging the roles of $x$ and $y$, and of $u$ and $v$.

An interesting interpretation of (2.1) arises from (A 21) (see also Morland 1987): the depth-integrated $xx$-component of (dimensional) stress is

$$\int_b^s -\rho g(s-z)+[\tau_{11}-P+\rho g(s-z)]\,\mathrm{d}z$$

in the original dimensional variables, where the first term is a hydrostatic contribution and the expression in square brackets is the effect of viscous stresses. At leading order in $\epsilon$, the contribution of viscous stresses is then

$$T_{11}=[\tau]\int_{\delta s^*-h^*}^{\delta s^*}\tau_{11}^*-P^*\,\mathrm{d}z^*=h(2\tau_{11}+\tau_{22})=Bhd^{p-2}(2\partial u/\partial x+\partial v/\partial y),$$

where we have re-introduced asterisks to distinguish dimensional and dimensionless variables. Similarly, the depth-integrated $xy$-component of dimensional stress is

$$T_{12}=[\tau]\int_{\delta s^*-h^*}^{\delta s^*}\tau_{12}^*\,\mathrm{d}z^*=h\tau_{12}=Bhd^{p-2}(\partial u/\partial y+\partial v/\partial z)$$

at leading order, and we may interpret (A 22) as a dimensionless version of

$$\frac{\partial T_{11}}{\partial x}+\frac{\partial T_{12}}{\partial y}-\rho gh\frac{\partial s}{\partial x}-\tau_c u/\sqrt{u^2+v^2}=0, \tag{A 23}$$

which is (2.7) with $i=1$. The boundary force in (2.10) can be calculated similarly.

### A.2. *No sliding: ice ridges*

No slip at the bed gives rise to an ordinary lubrication flow, provided the region of no slip has a low aspect ratio. This type of lubrication approximation, usually termed the *shallow ice approximation*, is discussed extensively in the literature (e.g. Morland & Johnson 1980; Baral, Hutter & Greve 2001), and we give only the relvant scalings here, so they can be compared with the corresponding scales for ice streams.

Suppose that the width scale of an ice ridge is $[x_\mathrm{r}]$, while the ice thickness scale is still $[h]$. This gives rise to a (small) aspect ratio parameter $\epsilon_\mathrm{r}=[h]/[x_\mathrm{r}]$, and appropriate scales $[u_\mathrm{r}]$ for horizontal velocities and $[\tau_\mathrm{r}]$ for shear stresses $\tau_{13}$ and $\tau_{23}$ are

$$[u_\mathrm{r}]=B^{-1/(p-1)}(\rho g\epsilon_\mathrm{r})^{1/(p-1)}[h]^{p/(p-1)},\qquad [\tau_\mathrm{r}]=\rho g[h]\epsilon_\mathrm{r} \tag{A 24}$$

https://doi.org/10.1017/S0022112006009591 Published online by Cambridge University Press

Moreover, stresses $\tau_{11}$, $\tau_{12}$ and $\tau_{22}$ scale with $\epsilon_r[\tau_r]$. The stress jump conditions between ridge and stream flow used in § 2.2 rely on these longitudinal and lateral shear stresses being small in ice ridges compared with ice streams (where they scale with $[\tau]$ as defined in § A.1), that is, on the condition $\epsilon_r[\tau_r]/[\tau] = \epsilon_r^2/\delta \ll 1$. Similarly, the velocity jump conditions rely on horizontal velocities in ice ridges being small compared with those in ice streams, or equivalently $[u_r]/[u] = \epsilon\epsilon_r^{1/(p-1)}/\delta^{1/(p-1)} \ll 1$. For small ridge and stream aspect ratios $\epsilon_r$ and $\epsilon$, this holds true provided the parameter $\delta$, measuring the ratio of surface elevation changes odsfdasfver distances $[x]$ in an ice stream relative to ice thickness, is not too small compared with $\epsilon$ and $\epsilon_r$ (and it certainly holds for $\delta = O(1)$).

Ice streams in West Antarctica have widths around $[x] \approx 50\,\mathrm{km}$, thicknesses $[h] \approx 1\,\mathrm{km}$ and surface slopes around $\theta \approx 10^{-3}$, which gives $\epsilon = 0.02$, $\delta = [s]/[h] = \theta[x]/[h] \approx 0.05$. The surrounding ice ridges also have widths around $[x_r] \approx 50\,\mathrm{km}$, so $\epsilon_r \approx 0.02$, and $\epsilon_r^2/\delta \approx 10^{-2}$. With $p = 4/3$ (based on $n = 3$ in Glen's law, see Paterson 1994, chapter 5), we also have $\epsilon\epsilon_r^{1/(p-1)}/\delta^{1/(p-1)} \approx 10^{-3}$, and numerically our assumptions about the various scales appear justified.

## Appendix B. Uniqueness and stability

In this Appendix, we discuss the uniqueness and stability (with respect to perturbations in ice thickness, basal friction and driving forces) of minimizers of the functional (3.13). We begin by defining an inner product $(\cdot,\cdot)$ and an associated norm $|\cdot|$ for real symmetric 2-by-2 matrices by

$$(\boldsymbol{A}, \boldsymbol{B}) = \frac{1}{2}\sum_{i,j=1}^{2}(A_{ij}B_{ij} + A_{ii}B_{jj}), \qquad |\boldsymbol{A}| = \sqrt{(\boldsymbol{A}, \boldsymbol{A})}. \tag{B 1}$$

From the usual properties of an inner product – which are easy to verify for $(\cdot,\cdot)$ – it can be shown that, for $1 < p \leqslant 2$,

$$(|\boldsymbol{A}| + |\boldsymbol{B}|)^{2-p}[|\boldsymbol{A}|^{p-2}(\boldsymbol{A}, \boldsymbol{A} - \boldsymbol{B}) + |\boldsymbol{B}|^{p-2}(\boldsymbol{B}, \boldsymbol{B} - \boldsymbol{A})] \geqslant C_p|\boldsymbol{A} - \boldsymbol{B}|^2, \tag{B 2}$$

where $C_p \geqslant (p-1)$ is a positive constant which depends only on $p$. Moreover, in a slight abuse of notation, we can write the variational inequality (3.7) as

$$\int_\Omega 2Bh|\boldsymbol{D}(\boldsymbol{u})|^{p-2}(\boldsymbol{D}(\boldsymbol{u}), \boldsymbol{D}(\boldsymbol{v}) - \boldsymbol{D}(\boldsymbol{u}))\,\mathrm{d}\Omega + \int_\Omega \tau_c(|\boldsymbol{v}| - |\boldsymbol{u}|) - \boldsymbol{f}\cdot(\boldsymbol{v} - \boldsymbol{u})\,\mathrm{d}\Omega - \int_{\partial\Omega}\boldsymbol{F}\cdot(\boldsymbol{v} - \boldsymbol{u})\,\mathrm{d}\Gamma \geqslant 0 \tag{B 3}$$

for all $\boldsymbol{v} \in [W^{1,p}(\Omega)]^2$. In addition, we will make use of the fact that

$$\int_\Omega |\boldsymbol{D}(\boldsymbol{v})|^p\,\mathrm{d}\Omega \leqslant 2^{p/2}\,\|\boldsymbol{v}\|^p$$

for $\boldsymbol{v} \in [W^{1,p}(\Omega)]^2$.

### B.1. *Uniqueness*

First we demonstrate that, if two distinct solutions $\boldsymbol{u}_1$ and $\boldsymbol{u}_2$ of (3.7) exist, they can only differ by a rigid body motion, $\boldsymbol{u}_2 - \boldsymbol{u}_1 = \boldsymbol{r}_\Delta \in \mathscr{R}$. Putting $\boldsymbol{u} = \boldsymbol{u}_1$, $\boldsymbol{v} = \boldsymbol{u}_2$ and vice versa in (B 3), and adding the resulting inequalities, we find

$$\int_\Omega 2Bh[|\boldsymbol{D}(\boldsymbol{u}_1)|^{p-2}(\boldsymbol{D}(\boldsymbol{u}_1), \boldsymbol{D}(\boldsymbol{u}_2) - \boldsymbol{D}(\boldsymbol{u}_1)) - |\boldsymbol{D}(\boldsymbol{u}_2)|^{p-2}(\boldsymbol{D}(\boldsymbol{u}_2), \boldsymbol{D}(\boldsymbol{u}_1) - \boldsymbol{D}(\boldsymbol{u}_2))]\,\mathrm{d}\Omega \geqslant 0. \tag{B 4}$$

https://doi.org/10.1017/S0022112006009591 Published online by Cambridge University Press

However, by (B 2), the integrand is always non-positive, and (B 4) can only hold if $\boldsymbol{D}(\boldsymbol{u}_2)-\boldsymbol{D}(\boldsymbol{u}_1)=\boldsymbol{D}(\boldsymbol{u}_2-\boldsymbol{u}_1)=\boldsymbol{0}$, from which it follows that $\boldsymbol{u}_2-\boldsymbol{u}_1\in\mathscr{R}$.

Since $J(\cdot)$ is convex and $\boldsymbol{u}_1$ and $\boldsymbol{u}_2$ are minimizers, any point on the straight line connecting $\boldsymbol{u}_1$ and $\boldsymbol{u}_2$ in $[W^{1,p}(\Omega)]^2$ must also be a minimizer. Hence we must have $J(\boldsymbol{u}_1)=J(\boldsymbol{u}_2)=J(\boldsymbol{u}_1+\lambda\boldsymbol{r}_\Delta)$ for all $\lambda\in[0,1]$. Using (3.13) and the fact that $\boldsymbol{D}(\boldsymbol{r}_\Delta)=\boldsymbol{0}$, we find

$$\int_\Omega \tau_c(|\boldsymbol{u}_1+\lambda\boldsymbol{r}_\Delta|-|\boldsymbol{u}_1|)\,\mathrm{d}\Omega=\lambda\left(\int_\Omega \boldsymbol{f}\cdot\boldsymbol{r}_\Delta\,\mathrm{d}\Omega+\int_{\partial\Omega}\boldsymbol{F}\cdot\boldsymbol{r}_\Delta\,\mathrm{d}\Gamma\right),\quad \lambda\in[0,1]. \tag{B 5}$$

Putting $\lambda=1$ and substituting the resulting expression for $\int_\Omega \boldsymbol{f}\cdot\boldsymbol{r}_\Delta\,\mathrm{d}\Omega+\int_{\partial\Omega}\boldsymbol{F}\cdot\boldsymbol{r}_\Delta\,\mathrm{d}\Gamma$ back in (B 5) yields

$$\int_\Omega \tau_c(|\boldsymbol{u}_1+\lambda\boldsymbol{r}_\Delta|-|\boldsymbol{u}_1|)\,\mathrm{d}\Omega=\lambda\int_\Omega \tau_c(|\boldsymbol{u}_1+\boldsymbol{r}_\Delta|-|\boldsymbol{u}_1|)\,\mathrm{d}\Omega,\qquad \lambda\in[0,1]. \tag{B 6}$$

Define $\Omega_\tau=\{(x_1,x_2)\in\Omega\,:\,\tau_c(x_1,x_2)>0\}$. It is then clear that $\int_\Omega \tau_c|\boldsymbol{u}_1+\lambda\boldsymbol{r}_\Delta|\,\mathrm{d}\Omega$ is strictly convex in $\lambda$, and hence that (B 5) cannot hold, unless $\boldsymbol{u}_1$ is parallel to $\boldsymbol{r}_\Delta$ almost everywhere in $\Omega_\tau$, that is, unless $\boldsymbol{u}_1(x_1,x_2)=\zeta(x_1,x_2)\boldsymbol{r}_\Delta(x_1,x_2)$ when $(x_1,x_2)\in\Omega_\tau$, where $\zeta$ is a scalar function which is smooth enough to ensure that $\zeta\boldsymbol{r}_\Delta$ is the restriction of some function in $[W^{1,p}(\Omega)]^2$ to the domain $\Omega_\tau$. When $\boldsymbol{u}_1$ is of this form, (B 6) becomes

$$\int_{\Omega_\tau} \tau_c|\boldsymbol{r}_\Delta|(|\lambda+\zeta|-|\zeta|)\,\mathrm{d}\Omega=\lambda\int_{\Omega_\tau} \tau_c|\boldsymbol{r}_\Delta|(|1+\zeta|-|\zeta|)\,\mathrm{d}\Omega,\qquad \lambda\in[0,1]. \tag{B 7}$$

There are then two cases to consider:

(i) There is a set $\Omega^\pm\subset\Omega_\tau$ of positive measure such that $\zeta(x_1,x_2)+\lambda$ changes sign as $\lambda$ varies over $(0,1)$ for all $(x_1,x_2)\in\Omega^\pm$. In that case, $\tau_c|\boldsymbol{r}_\Delta|(|\lambda+\zeta(x_1,x_2)|-|\zeta(x_1,x_2)|)<\tau_c|\boldsymbol{r}_\Delta|\lambda(|1+\zeta(x_1,x_2)|-|\zeta(x_1,x_2)|)$ for $(x_1,x_2)\in\Omega^\pm$, $\lambda\in(0,1)$. Hence

$$\int_{\Omega_\tau} \tau_c|\boldsymbol{r}_\Delta|(|\lambda+\zeta|-|\zeta|)\,\mathrm{d}\Omega<\lambda\int_{\Omega_\tau}(\tau_c|\boldsymbol{r}_\Delta|(|1+\zeta|-|\zeta|))\,\mathrm{d}\Omega,\qquad \lambda\in(0,1) \tag{B 8}$$

which contradicts (B 7).

(ii) $\zeta(x_1,x_2)+\lambda$ remains of the same sign for all $(x_1,x_2)\in\Omega_\tau$ as $\lambda$ varies over $(0,1)$ (except possibly for $(x_1,x_2)$ in a subset of measure zero, which we can avoid by re-defining $\zeta$ on that set). Define $\Omega^+=\{(x_1,x_2)\in\Omega_\tau\,:\,\zeta(x_1,x_2)\geqslant 0\}$, $\Omega^-=\{(x_1,x_2)\in\Omega_\tau\,:\,\zeta(x_1,x_2)\leqslant -1\}$, such that $\Omega_\tau=\Omega^+\cup\Omega^-$. Then (B 5) takes the form

$$\int_{\Omega^+}\tau_c|\boldsymbol{r}_\Delta|\,\mathrm{d}\Omega-\int_{\Omega^-}\tau_c|\boldsymbol{r}_\Delta|\,\mathrm{d}\Omega=\int_\Omega \boldsymbol{f}\cdot\boldsymbol{r}_\Delta\,\mathrm{d}\Omega+\int_{\partial\Omega}\boldsymbol{F}\cdot\boldsymbol{r}_\Delta\,\mathrm{d}\Gamma, \tag{B 9}$$

which serves as a necessary condition for non-uniqueness. Note that (B 9) cannot hold if $\zeta$ is of one sign in $\Omega_\tau$, in which case either $\Omega^+=\varnothing$ and (3.15) does not hold with $\boldsymbol{r}=-\boldsymbol{r}_\Delta$, or $\Omega^-=\varnothing$ and (3.15) does not hold with $\boldsymbol{r}=\boldsymbol{r}_\Delta$.

It is also straightforward to show that the results above provide a sufficient condition for non-uniqueness. Specifically, a solution $\boldsymbol{u}$ is non-unique if it takes the form $\boldsymbol{u}=\zeta\boldsymbol{r}_\Delta\not\equiv 0$ on $\Omega_\tau$ for some $\boldsymbol{r}_\Delta\in\mathscr{R}$ and a sufficiently smooth scalar function $\zeta$, provided $\zeta$ allows $\Omega_\tau$ to be decomposed into $\Omega^+$ and $\Omega^-$ as above such that (B 9) holds. We note that these conditions for non-uniqueness are quite specialized, and for most arbitrarily chosen combinations of the data functions $h$, $\tau_c$, $\boldsymbol{f}$ and $\boldsymbol{F}$, we may expect them not to be satisfied.

One further interesting result arises as follows: suppose that multiple solutions do exist as described above. Then, for any $\lambda\in(0,1)$, $\zeta+\lambda\neq 0$ on $\Omega_\tau$, as $\zeta+\lambda$ would

https://doi.org/10.1017/S0022112006009591 Published online by Cambridge University Press

otherwise change sign for that value of $\lambda$. Then the solution $\boldsymbol{u}_\lambda = \boldsymbol{u}_1 + \lambda \boldsymbol{r}_\Delta$ is of the form $\boldsymbol{u}_\lambda = (\zeta + \lambda)\boldsymbol{r}_\Delta$ on $\Omega_\tau$, and therefore non-zero almost everywhere in $\Omega_\tau$, and, when the velocity field takes the form $\boldsymbol{u}_\lambda$, sliding occurs almost everywhere in the region where friction is non-zero.

### B.2. *Stability*

We briefly consider the stability of solutions to perturbations in ice thickness $h$, yield stress $\tau_c$ and gravitational forces $\boldsymbol{f}$ and $\boldsymbol{F}$. Suppose that $\boldsymbol{u}_1$, $\boldsymbol{u}_2$ satisfy the variational inequalities (where $i = 1, 2$)

$$\int_\Omega 2Bh_i|\boldsymbol{D}(\boldsymbol{u}_i)|^{p-2}(\boldsymbol{D}(\boldsymbol{u}_i), \boldsymbol{D}(\boldsymbol{v}) - \boldsymbol{D}(\boldsymbol{u}_i))\,\mathrm{d}\Omega + \int_\Omega \tau_i(|\boldsymbol{v}| - |\boldsymbol{u}_i|) - \boldsymbol{f}_i \cdot (\boldsymbol{v} - \boldsymbol{u}_i)\,\mathrm{d}\Omega - \int_{\partial\Omega} \boldsymbol{F}_i \cdot (\boldsymbol{v} - \boldsymbol{u}_i)\,\mathrm{d}\Gamma \geqslant 0 \quad \text{(B 10)}$$

for all $\boldsymbol{v} \in [W^{1,p}(\Omega)]^2$. Consider now the case $\|h_2 - h_1\| \to 0$, $\|\tau_2 - \tau_1\| \to 0$, $\|\boldsymbol{f}_2 - \boldsymbol{f}_1\| \to 0$, $\|\boldsymbol{F}_2 - \boldsymbol{F}_1\| \to 0$ with $h_1$, $\tau_1$, $\boldsymbol{f}_1$ and $\boldsymbol{F}_1$ fixed. Suppose also that $\tau_2$, $\boldsymbol{f}_2$ and $\boldsymbol{F}_2$ are such that (3.15) is satisfied uniformly for some constant $\delta_{\mathscr{R}} > 0$, and that $h_2 > h_0$ almost everywhere uniformly for some constant $h_0$; it then follows from § 3.1 that $\|\boldsymbol{u}_2\|$ and $\|\boldsymbol{u}_1\|$ exist and are bounded above uniformly by some $R_0 > 0$.

Putting $i = 1$, $\boldsymbol{v} = \boldsymbol{u}_2$, and $i = 2$, $\boldsymbol{v} = \boldsymbol{u}_1$ in (B 10) yields

$$\int_\Omega 2Bh_1|\boldsymbol{D}(\boldsymbol{u}_1)|^{p-2}(\boldsymbol{D}(\boldsymbol{u}_1), \boldsymbol{D}(\boldsymbol{u}_2) - \boldsymbol{D}(\boldsymbol{u}_1))\,\mathrm{d}\Omega + \int_\Omega \tau_1(|\boldsymbol{u}_2| - |\boldsymbol{u}_1|) - \boldsymbol{f}_1 \cdot (\boldsymbol{u}_2 - \boldsymbol{u}_1)\,\mathrm{d}\Omega - \int_{\partial\Omega} \boldsymbol{F}_1 \cdot (\boldsymbol{u}_2 - \boldsymbol{u}_1)\,\mathrm{d}\Gamma \geqslant 0, \quad \text{(B 11)}$$

$$\int_\Omega 2Bh_2|\boldsymbol{D}(\boldsymbol{u}_2)|^{p-2}(\boldsymbol{D}(\boldsymbol{u}_2), \boldsymbol{D}(\boldsymbol{u}_1) - \boldsymbol{D}(\boldsymbol{u}_2))\,\mathrm{d}\Omega + \int_\Omega \tau_2(|\boldsymbol{u}_1| - |\boldsymbol{u}_2|) - \boldsymbol{f}_2 \cdot (\boldsymbol{u}_1 - \boldsymbol{u}_2)\,\mathrm{d}\Omega - \int_{\partial\Omega} \boldsymbol{F}_2 \cdot (\boldsymbol{u}_1 - \boldsymbol{u}_2)\,\mathrm{d}\Gamma \geqslant 0. \quad \text{(B 12)}$$

Adding these two inequalities yields after some manipulation using Hölder's inequality

$$\int_\Omega 2Bh_1[|\boldsymbol{D}(\boldsymbol{u}_1)|^{p-2}(\boldsymbol{D}(\boldsymbol{u}_1), \boldsymbol{D}(\boldsymbol{u}_1) - \boldsymbol{D}(\boldsymbol{u}_2)) - |\boldsymbol{D}(\boldsymbol{u}_2)|^{p-2}(\boldsymbol{D}(\boldsymbol{u}_2), \boldsymbol{D}(\boldsymbol{u}_1) - \boldsymbol{D}(\boldsymbol{u}_2))]\,\mathrm{d}\Omega \leqslant 2^{2+p/2}B\,\|h_2 - h_1\|\,R_0^p + 2\,\|\tau_2 - \tau_1\|\,R_0 + 2\,\|\boldsymbol{f}_1 - \boldsymbol{f}_2\|\,R_0 + 2C_2\,\|\boldsymbol{F}_1 - \boldsymbol{F}_2\|\,R_0 \doteq \Delta, \quad \text{(B 13)}$$

where $C_2$ is again the norm of the trace operator from $[W^{1,p}(\Omega)]^2$ into $[L^p(\partial\Omega)]^2$. Use of (B 2) as well as Hölder's inequality then leads to (see also Fernandez Bonder & Rossi 2001; Schoof 2006)

$$(2Bh_0C_p)^{p/2} \int_\Omega |\boldsymbol{D}(\boldsymbol{u}_2 - \boldsymbol{u}_1)|^p\,\mathrm{d}\Omega \leqslant \left(2^{1+1/2}R_0\right)^{(2-p)p/2}\Delta^{p/2}, \quad \text{(B 14)}$$

where $\Delta$ is defined on the last line of (B 13).

Define $\boldsymbol{w} = \boldsymbol{u}_2 - \boldsymbol{u}_1$. As in (3.16), we can decompose $\boldsymbol{w}$ into a rotational part $\boldsymbol{w}_{\mathscr{R}}$ and a remainder $\tilde{\boldsymbol{w}}$. Using Korn's second inequality, (B 14) immediately proves that $\|\tilde{\boldsymbol{w}}\|$ tends to zero as the data function perturbations represented by $\Delta$ do:

$$(2Bh_0C_p)^{p/2}C_1\,\|\tilde{\boldsymbol{w}}\|^p \leqslant \left(2^{1+1/2}R_0\right)^{(2-p)p/2}\Delta^{p/2}, \quad \text{(B 15)}$$

https://doi.org/10.1017/S0022112006009591 Published online by Cambridge University Press

where $C_1$ is the same constant as in § 3.1. In order to show the stability of solutions to perturbations in the data functions, it remains to show that $\boldsymbol{w}_{\mathscr{R}}$ also tends to zero as perturbations in the data functions do. Naturally, this is only possible if $\boldsymbol{u}_1$ is indeed unique, so we suppose this to be the case.

From (B 12) we find after some manipulation that

$$\int_\Omega \tau_2(|\boldsymbol{u}_1| - |\boldsymbol{u}_1 + \boldsymbol{w}_{\mathscr{R}}|) + \boldsymbol{f}_2 \cdot \boldsymbol{w}_{\mathscr{R}} \,\mathrm{d}\Omega + \int_{\partial\Omega} \boldsymbol{F}_2 \cdot \boldsymbol{w}_{\mathscr{R}} \,\mathrm{d}\Gamma \geqslant -\left(2^{1+p/2} B \,\|h_2\|\, R_0^{p-1} + \|\tau_2\| + \|\boldsymbol{f}_2\| + \|\boldsymbol{F}_2\|\right) \|\tilde{\boldsymbol{w}}\|, \quad \text{(B 16)}$$

or

$$\begin{aligned}\int_\Omega \tau_1(|\boldsymbol{u}_1 + \boldsymbol{w}_{\mathscr{R}}| - |\boldsymbol{u}_1|) - \boldsymbol{f}_1 \cdot \boldsymbol{w}_{\mathscr{R}} \,\mathrm{d}\Omega - \int_{\partial\Omega} \boldsymbol{F}_1 \cdot \boldsymbol{w}_{\mathscr{R}} \,\mathrm{d}\Gamma \\ \leqslant \left(2^{1+p/2} B \,\|h_2\|\, R_0^{p-1} + \|\tau_2\| + \|\boldsymbol{f}_2\| + \|\boldsymbol{F}_2\| + \|\tau_2 - \tau_1\| + \|\boldsymbol{f}_2 - \boldsymbol{f}_1\| + \|\boldsymbol{F}_2 - \boldsymbol{F}_1\|\right) \|\tilde{\boldsymbol{w}}\| \\ + 2\,\|\tau_2 - \tau_1\|\, R_0 + 2\,\|\boldsymbol{f}_2 - \boldsymbol{f}_1\|\, R_0 + 2\,\|\boldsymbol{F}_2 - \boldsymbol{F}_1\|\, R_0 \doteq \nu, \quad \text{(B 17)}\end{aligned}$$

where, by the results above, $\nu$ defined on the last line tends to zero as perturbations in the data functions tend to zero.

Consider the continuous functional $\phi : \mathscr{R} \mapsto \mathbb{R}$ defined by

$$\phi(\boldsymbol{r}) = \int_\Omega \tau_1(|\boldsymbol{u}_1 + \boldsymbol{r}| - |\boldsymbol{u}_1|) - \boldsymbol{f}_1 \cdot \boldsymbol{r} \,\mathrm{d}\Omega - \int_{\partial\Omega} \boldsymbol{F}_1 \cdot \boldsymbol{r} \,\mathrm{d}\Gamma, \quad \text{(B 18)}$$

and let

$$\Phi(r) = \min_{\boldsymbol{r} \in \mathscr{R} : \|\boldsymbol{r}\| = r} \phi(\boldsymbol{r}) \quad \text{(B 19)}$$

for $r \in [0, \infty)$. It is straightforward to show that $\Phi$ is also continuous on $[0, \infty)$, and (B 17) implies that

$$\Phi(\|\boldsymbol{w}_{\mathscr{R}}\|) \leqslant \phi(\boldsymbol{w}_{\mathscr{R}}) \leqslant \nu. \quad \text{(B 20)}$$

Now, since $\boldsymbol{u}_1$ uniquely minimizes the functional

$$J_1(\boldsymbol{v}) = \int_\Omega \frac{2Bh_1}{p} |\boldsymbol{D}(\boldsymbol{v})|^p + \tau_1 |\boldsymbol{v}| - \boldsymbol{f}_1 \cdot \boldsymbol{v} \,\mathrm{d}\Omega - \int_{\partial\Omega} \boldsymbol{F}_1 \cdot \boldsymbol{v} \,\mathrm{d}\Gamma, \quad \text{(B 21)}$$

we have, for $\boldsymbol{r} \in \mathscr{R}$, that $J_1(\boldsymbol{u}_1 + \boldsymbol{r}) - J_1(\boldsymbol{u}_1) = \phi(\boldsymbol{r}) > 0$ provided $\boldsymbol{r} \neq \boldsymbol{0}$. Since $\mathscr{R}$ is finite-dimensional, it follows that $\Phi(r) > 0$ when $r > 0$ (with $\Phi(0) = 0$), and furthermore, since $\phi$ is convex, we can show that $\Phi$ must be an increasing function. Hence, by (B 20) and the continuity of $\Phi$, we have that $\|\boldsymbol{w}_{\mathscr{R}}\| \to 0$ as $\nu \to 0$, the rate of convergence being determined by the exact behaviour of the function $\Phi$.

## REFERENCES


Alley, R. B. & Bindschadler, R. A. (Eds.) 2001 *The West Antarctic Ice Sheet: Behaviour and Environment*. American Geophysical Union.

Baral, D. R., Hutter, K. & Greve, R. 2001 Asymptotic theories of large-scale motion, temperature distribution in land-based polythermal ice sheets: A critical review and new developments. *Appl. Mech. Rev.* **54** (3), 215–256.

Blatter, H. 1995 Velocity and stress fields in grounded glaciers – a simple algorithm. *J. Glaciol.* **41** (138), 333–344.

Colinge, J. & Blatter, H. 1998 Stress and velocity fields in glaciers: Part I. Finite-difference schemes for higher-order glacier models. *J. Glaciol.* **44** (148), 448–456.

Dennis, J. E. & Schnabel, R. B. 1996 *Numerical Methods for Unconstrained Optimization and Nonlinear Equations*. SIAM.


https://doi.org/10.1017/S0022112006009591 Published online by Cambridge University Press

Duvaut, G. & Lions, J. L. 1976 *Inequalities in Mechanics and Physics*. Springer.

Ekeland, I. & Temam, R. 1976 *Convex Analysis and Variational Problems*. North-Holland.

Engelhardt, H. & Kamb, B. 1997 Basal hydraulic system of a West Antarctic ice stream: constraints from borehole observations. *J. Glaciol.* **43** (144), 207–230.

Evans, L. C. 1998 *Partial Differential Equations*. American Mathematical Society.

Fernandez Bonder, J. & Rossi, J. D. 2001 Existence results for the $p$-Laplacian with nonlinear boundary conditions. *J. Math. Anal. Appl.* **263**, 195–223.

Fowler, A. C. & Johnson, C. 1996 Ice-sheet surging and ice-stream formation. *Ann. Glaciol.* **23**, 68–73.

Goldsby, D. L. & Kohlstedt, D. L. 2001 Superplastic deformation of ice: Experimental observations. *J. Geophys. Res.* **106** (B6), 11017–11030.

Joughin, I., MacAyeal, D. R. & Tulaczyk, S. 2004 Basal shear stress of the Ross ice streams from control method inversions. *J. Geophys. Res.* **109** (B09405), doi:10.1029/2003JB002960.

Kikuchi, N. & Oden, J. T. 1988 *Contact Problems in Elasticity: A Study of Variational Inequalities and Finite Element Methods*. SIAM.

MacAyeal, D. R. 1987 Ice-shelf backpressure: form drag versus dynamics drag. In *Dynamics of the West Antarctic Ice Sheet. Proc. Workshop held in Utrecht, May 6–8, 1985* (ed. C. J. van der Veen & J. Oerlemans), pp. 141–160. D. Reidel.

MacAyeal, D. R. 1989 Large-scale flow over a viscous basal sediment: theory and application to Ice Stream E, Antarctica. *J. Geophys. Res.* **94** (B4), 4017–4087.

MacAyeal, D. R. 1996 EISMINT: Lessons in Ice-Sheet Modeling. *Tech. Rep.* Department of Geophysical Sciences, University of Chicago, unpublished lecture notes.

Morland, L. W. 1987 Unconfined ice-shelf flow. In *Dynamics of the West Antarctic Ice Sheet. Proc. Workshop held in Utrecht, May 6–8, 1985* (ed. C. J. van der Veen & J. Oerlemans), pp. 99–116. D. Reidel.

Morland, L. W. & Johnson, I. R. 1980 Steady motion of ice sheets. *J. Glaciol.* **25** (92), 229–246.

Morland, L. W. & Zainuddin, R. 1987 Plane and radial ice-shelf flow with prescriped temperature profile. In *Dynamics of the West Antarctic Ice Sheet. Proc. Workshop held in Utrecht, May 6–8, 1985* (ed. C. J. van der Veen & J. Oerlemans), pp. 117–140. D. Reidel.

Paterson, W. S. B. 1994 *The Physics of Glaciers*, 3rd Edn. Pergamon.

Picasso, M., Rappaz, J., Reist, A., Funk, M. & Blatter, H. 2004 Numerical simulation of the motion of a glacier. *Intl J. Numer. Meth. Engng* **5**, 995–1009.

Retzlaff, R. & Bentley, C. R. 1993 Timing of stagnation of Ice Stream C, West Antarctica, from short-pulse radar studies of buried crevasses. *J. Glaciol.* **39** (133), 553–561.

Rignot, E., Cassassa, G., Gogineni, S., Krabill, W., Rivera, A. & Thomas, R. 2004 Accelerated ice discharge from the Antarctic Peninsula following the collapse of Larsen B ice shelf. *Geophys. Res. Lett.* **31** (18), L18401, doi:10.1029/2004GL020697.

Schmeltz, M., Rignot, E., Dupont, T. K. & MacAyeal, D. R. 2002 Sensitivity of Pine Island Glacier, West Antarctica, to changes in ice-shelf and basal conditions: a model study. *J. Glaciol.* **48** (163), 552–558.

Schoof, C. 2004 On the mechanics of ice stream shear margins. *J. Glaciol.* **50** (169), 208–218.

Schoof, C. 2006 Variational methods for glacier flow over plastic till. *J. Fluid Mech.* **555**, 299–320.

Shumskiy, P. A. & Krass, M. S. 1976 Mathematical models of ice shelves. *J. Glaciol.* **17**, 419–432.

Tulaczyk, S. 1999 Ice sliding over weak, fine-grained till: dependence of ice-till interactions on till granulometry. *Spec. Paper Geol. Soc. Am.* **337**, 159–177.

Tulaczyk, S., Kamb, W. B. & Engelhardt, H. F. 2000 Basal mechanisms of Ice Stream B, West Antarctica: 2. Undrained plastic bed model. *J. Geophys. Res.* **105** (B1), 483–494.

van der Veen, C. J. & Whillans, I. M. 1996 Model experiments on the evolution and stability of ice streams. *Ann. Glaciol.* **23**, 129–137.

Wang, L. H. 2003 On Korn's inequality. *J. Comput. Math* **21** (3), 321–324.

Whillans, I. M. & van der Veen, C. J. 1997 The role of lateral drag in the dynamics of Ice Stream B, Antarctica. *J. Glaciol.* **43** (144), 231–237.

https://doi.org/10.1017/S0022112006009591 Published online by Cambridge University Press